AMT-562, a Novel HER3-targeting Antibody–Drug Conjugate, Demonstrates a Potential to Broaden Therapeutic Opportunities for HER3-expressing Tumors

Weining Weng[1,2], Tao Meng[3,4], Junyi Pu[5], Linjie Ma[2], Yi Shen[2], Zhaohui Wang[6], Rong Pan[6], Mingqiao Wang[6], Caiwei Chen[2], Lijun Wang[2], Jianjian Zhang[2], Biao Zhou[2], Siyuan Shao[7], Yu Qian[1], Shuhui Liu[2], Wenhao Hu[1], and Xun Meng[2,6]

ABSTRACT

HER3 is a unique member of the EGFR family of tyrosine kinases, which is broadly expressed in several cancers, including breast, lung, pancreatic, colorectal, gastric, prostate, and bladder cancers and is often associated with poor patient outcomes and therapeutic resistance. U3-1402/Patritumab-GGFG-DXd is the first successful HER3-targeting antibody–drug conjugate (ADC) with clinical efficacy in non–small cell lung cancer. However, over 60% of patients are nonresponsive to U3-1402 due to low target expression levels and responses tend to be in patients with higher target expression levels. U3-1402 is also ineffective in more challenging tumor types such as colorectal cancer. AMT-562 was generated by a novel anti-HER3 antibody Ab562 and a modified self-immolative PABC spacer (T800) to conjugate exatecan. Exatecan showed higher cytotoxic potency than its derivative DXd. Ab562 was selected because of its moderate affinity for minimizing potential toxicity and improving tumor penetration purposes. Both alone or in combination therapies, AMT-562 showed potent and durable antitumor response in low HER3 expression xenograft and heterogeneous patient-derived xenograft/organoid models, including digestive system and lung tumors representing of unmet needs. Combination therapies pairing AMT-562 with therapeutic antibodies, inhibitors of CHEK1, *KRAS*, and tyrosine kinase inhibitor showed higher synergistic efficacy than Patritumab-GGFG-DXd. Pharmacokinetic and safety profiles of AMT-562 were favorable and the highest dose lacking severe toxicity was 30 mg/kg in cynomolgus monkeys. AMT-562 has potential to be a superior HER3-targeting ADC with a higher therapeutic window that can overcome resistance to generate higher percentage and more durable responses in U3-1402–insensitive tumors.

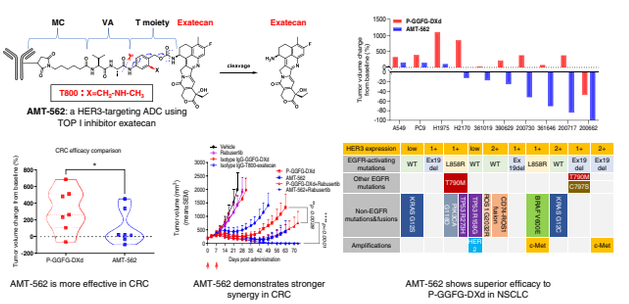

Introduction

HER3 is a unique member of the EGFR family of tyrosine kinases (ErbB; refs. 1, 2). It is a pseudokinase lacking significant kinase activity and requires heterodimerization with other members of ErbB family to activate downstream signaling pathways (1, 3, 4). HER3 is broadly expressed in solid tumors such as breast, lung, pancreatic, colorectal, gastric, prostate, and bladder cancers and is often associated with poor patient outcomes and therapeutic resistance (5–8). These observations have resulted in the development of therapeutic agents for HER3-expressing breast cancer and other solid tumors (1). The classical ATP-analog class of tyrosine kinase inhibitors (TKI) is not effective against HER3 because enzymatic catalytic activity do not mediate its function. HER3 can only be blocked by targeting its extracellular domain (ECD) with specific antibodies (9). However, functional mAbs against HER3, such as patritumab (U3-1287) or dual-target mAbs against EGFR/HER3, such as duligotuzumab, have not shown significant clinical benefit (10, 11).

Antibody–drug conjugates (ADC) are a class of biopharmaceutical drugs designed for cancer therapy, in which antibodies specific for cell surface tumor-associated antigens selectively deliver cytotoxic drugs conjugated to antibodies via synthetic linkers to tumor cells (12). The antitumor activity of ADCs is not necessarily dependent on the drug's ability to inhibit downstream oncogenic driver signaling pathways, but rather on target expression, internalization rate, intracellular trafficking, and recycling rate which representing a fundamentally different targeted cancer therapy strategy. Patritumab deruxtecan (Patritumab-GGFG-DXd or HER3-DXd or U3-1402) is a potential first-in-class HER3-directed ADC (13–16). U3-1402 comprises patritumab linked to a potent topoisomerase I (Top I) inhibitor DXd via a tetrapeptide linker GGFG. In the clinical setting, patritumab deruxtecan demonstrates safety and promising antitumor efficacy in patients with heavily pretreated HER3-expressing metastatic breast cancer and EGFR-mutated non–small cell lung cancer (NSCLC; refs. 17–19).

[1]Guangdong Key Laboratory of Chiral Molecule and Drug Discovery, School of Pharmaceutical Sciences, Sun Yat-sen University, Guangzhou, P.R. China. [2]Multitude Therapeutics, Shanghai, P.R. China. [3]MabCare Therapeutics, Shanghai, P.R. China. [4]HySlink Therapeutics, Shanghai, P.R. China. [5]School of Life Sciences, Northwest University, Xi'an, Shaanxi, P.R. China. [6]Abmart Inc, Shanghai, P.R. China. [7]Shanghai OneTar Biomedicine, Shanghai, P.R. China.

Corresponding Authors: Xun Meng, Multitude Therapeutics, 3rd floor Building 1, 333 Guiping Road, Shanghai 200233, P.R. China. Phone: 8602-1540-19129; E-mail: xun.meng@multitudetherapeutics.com; and Wenhao Hu, Sun Yat-sen University, Guangzhou, 510006, P.R. China. Phone: 8613-6322-26060; E-mail: huwh9@mail.sysu.edu.cn

Mol Cancer Ther 2023;22:1013–27

doi: 10.1158/1535-7163.MCT-23-0198

Despite U3-1402's potential to become the first approved HER3-targeting ADC, 60% of patients with EGFR-mutated NSCLC fail to respond to U3-1402 therapy due to low expression rate of HER3 target, while patients with higher HER3 expression tend to have better responses (19). These results are similar to HER2-targeting ADCs T-DM1 (20, 21) or T-DXd (22, 23), or Nectin-4–targeting ADC enfortumab vedotin (24), which all demonstrate a positive correlation between target expression level and patient response. In patients with NSCLC without an EGFR mutation, the patient response rate was lower (less than 30%) due to the lower expression level of HER3 in those patients compared with patients with EGFR-mutated, TKI-resistant NSCLC. This clinical performance is consistent with U3-402's preclinical efficacy data in which it inhibits cell/tumor growth activity in HER3-high expression but is much less effective in HER3-low models (13–16). In breast and colon cancer models, U3-1402 efficacy is associated with high baseline HER3 expression (14, 15). In a preclinical study targeting prostate cancer, U3-1402 showed limited antitumor activity in the HER3-low model *in vitro* and *in vivo* compared with strong antitumor efficacy for high HER3 expression models (25), further reenforcing this pattern. A HER3-targeting ADC with an improved therapeutic index in U3-1402–insensitive tumors, including low-HER3 expression lung cancer or colon cancer, will likely expand responding patient population and applicable tumor types to realize the full potential of HER3 as a tumor antigen broadly overexpressed in solid tumors.

We have recently introduced a class of ADCs, T moiety–exatecan conjugates, which demonstrate an improved therapeutic index and favorable safety profile (26). T moiety–exatecan ADCs show improved stability and potency, stronger bystander killing effect, deeper and more durable intratumoral pharmacodynamic response due to their superior payload features and T moiety chemistry. Exatecan, the precursor of DXd, is higher potency, less sensitive to multi-drug resistance (MDR), and has higher cell permeability for a stronger bystander killing effect compared with DXd (26, 27). Exatecan was conjugated to antibodies through a novel, hydrophilic self-immolative T moiety (T800 or T1000) to overcome exatecan's high hydrophobicity (26). Using patritumab, T moiety–exatecan antibody conjugate P-T moiety-exatecan displayed improved antitumor efficacy compared with P-GGFG-DXd, especially in low HER3 and high MDR expression tumors (26). Here we have employed a more holistic approach in designing and characterizing a novel HER3-targeting ADC, AMT-562, for clinical investigation. Antibody selection was based on HER3 biology and optimal T moiety was selected with a balanced consideration of ADC potency and safety. Consequently, a highly hydrophilic, functional HER3-targeting antibody Ab562 of a medium affinity was paired with the moderately hydrophilic T800 structure to yield AMT-562 with high potency and low toxicity. The cytotoxic activity of AMT-562 in HER3-expressing cells was mediated by released exatecan through DNA damage and apoptosis induction. AMT-562 produced deeper and more durable antitumor responses in low-target expression cell line and patient-derived xenograft (PDX) models of pancreatic, esophagus, colon, and gastric cancer, including ones resistant to Patritumab-GGFG-DXd. In colon cancer cells, AMT-562 showed synergistic efficacy and synthetic lethality with inhibitors of DNA-damaging pathway mediator CHEK1, VEGF, and EGFR. In lung cancer with different EGFR TKI inhibitor resistant mechanisms and wild-type EGFR, AMT-562 outperformed Patritumab-GGFG-DXd alone or in combination with TKI or a *KRAS* G12C inhibitor, especially in low HER3 expression tumors. AMT-562 has the potential to induce superior antitumor activity compared with Patritumab-GGFG-DXd (U3-1402) and is entering clinical investigation in HER3-expressing solid tumors.

Materials and Methods

mAb562 isolation

Six to 8 weeks old female BALB/c mice were used for an immunization process and injected with antigenic peptides were injected six times. One day after the final immunization, total splenocytes were isolated and fused with the myeloma cell line SP2/0 (ATCC), utilizing PEG for cell fusion and HAT medium for hybridomas selection. After 7 to 10 days, single hybridoma clones were isolated and antibody-producing hybridomas were selected by screening supernatants for antigen binding using ELISA. All positive clones were injected into mice for ascites generation. Ascites were purified in protein A/G (MabSelect, GE Healthcare Life Sciences) gravity columns and screened again using flow cytometry. One clone, mAb562, was selected for subsequent sequencing, humanization, and further development into the final antibody Ab562.

Antibodies, ADCs, and compounds

Herceptin (trastuzumab), cetuximab, and bevacizumab were all purchased from Geneway Bio-Technology Co., Ltd., anti-HER3 humanized antibodies (patritumab and Ab562) were generated in CHO expression system and purified by MabSelect Sure Resin (GE Healthcare Life Sciences) in gravity columns. The sequence of patritumab was obtained from the corresponding patents and literatures. Isotype IgG was purchased from Beijing Solarbio Science & Technology Co., Ltd. ADCs were synthesized as described below and their drug-to-antibody ratio (DAR) values were determined by reverse-phase chromatography. The drug distribution was analyzed by hydrophobic interaction chromatography (HIC). P-GGFG-DXd (U3-1402) was made in-house using linker-payloads directly purchased from MedChemExpress: MC-GGFG-DXd (HY-114233, MedChemExpress). Exatecan (HY-13631), DXd (HY-13631E), AZD9291 (HY-15772), Rabusertib (HY-14720), Gefitinib (HY-50895), and Sotorasib (HY-114277) were all purchased from MedChemExpress.

ADC preparation

A solution of naked mAb [10 mg/mL in PBS (7.0) + 2 mmol/L ethylenediaminetetraacetic acid (EDTA)] was treated with 7 molar equivalents of tris(2-carboxyethyl)phosphine for 2 hours at 37°C. Then 14 molar equivalents of linker-drug (from a 10 mmol/L N,N-dimethylacetamide (DMA) stock solution) were added to the fully reduced antibody, while the residual DMA concentration was kept below 10% (v/v). The mixture was incubated at room temperature for an hour followed by purification over a zeba spin desalting column (Thermo Fisher Scientific) to remove excess reagents. In this step, the resulting ADC was also buffer exchanged into formulation buffer (20 mmol/L histidine, 150 mmol/L NaCl, pH 5.5). Moreover, the excess linker-drug could be removed thoroughly by treating the product with activated charcoal (30 mg of charcoal to 1 mL ADC solution) followed by 2 hours of vortexing at room temperature. The charcoal was then removed via sterile filtration (0.2 μmol/L PES filters) and the final ADC was stored at −80°C.

ADC concentration, DAR, and aggregation measurement

The concentration of mAb and the conjugated drug in the ADC were calculated by measuring UV absorbance of an aqueous solution in the ADC at two wavelengths, 280 nm and 370 nm, because the total absorbance at any given wavelength is equal to the sum of the absorbance of all light-absorbing chemical species that are present in a system (additivity of absorbance). Equations were as follows. $A280 = AD,280 + AA,280 = \varepsilon D,280CD + \varepsilon A,280CA$ (1), and $A370 = AD,370 + AA,370 = \varepsilon D,370CD + \varepsilon A,370CA$ (2). The values of εA,280, εA,370, εD,280, and εD,370 were estimated on the basis of

calculating the amino acid sequence of the antibody or obtained by UV measurement of the compound according to Lambert–Beer law. The simultaneous equations (1) and (2) were solved by substitution of above values, and then CA and CD were determined. Dividing CD by CA determined the average number of conjugated drug molecules per antibody.

Aggregation was assessed by size exclusion chromatography, which was performed on an Agilent 1260 Infinity II High-performance liquid chromatography (HPLC) system with UV detection at 280 nm. The column was a TSKgel G3000SWXL column (Tosoh Bioscience). Samples were injected at 50 μg load. Mobile phase was consisted of 200 mmol/L sodium phosphate and 150 mmol/L sodium chloride (pH 7.0). Also, 15% (v/v) isopropanol was added to the mobile phase to minimize secondary hydrophobic interactions with the stationary phase and furthermore prevent bacterial growth. Flow rate was 0.75 mL/minute and the column temperature was set at room temperature.

ADCs with different number of drugs per antibody were separated using a butyl HIC column (TSK-gel Butyl-NPR 4.6 × 35 mm 2.5 μm, Tosoh Bioscience) and LC/MS, respectively. HIC was also performed on an Agilent 1260 Infinity II HPLC system with UV detection at 280 nm. Mobile phase A was 1.5 M $(NH_4)_2SO_4$, 50 mmol/L K_2HPO_4, pH7.0 and mobile phase B was 21.3 mmol/L KH_2PO_4, 28.6 mmol/L K_2HPO_4, 25% (v/v) isopropanol, pH7.0. Gradient program was as follows. B %: 0%–25% (0 minute–1 minute, 0.8 mL/minute), 25% (1 minute–3 minutes, 0.6 mL/minute), 25%–80% (3 minutes–13 minutes, 0.6 mL/minute), 80% (13 minutes–17 minutes, 0.6 mL/minute), 80%–0% (17 minute–17.10 minutes, 0.5 mL/minute), 0% (17.10 minutes–25 minutes, 0.7 mL/minute).

Cell lines and PDX models

SK-BR-3 (RRID: CVCL_0033), SNU-16 (RRID: CVCL_0076), SW620 (RRID: CVCL_0547), COLO205 (RRID: CVCL_0218), HCT-15 (RRID: CVCL_0292), COLO320DM (RRID: CVCL_0219), AsPC-1 (RRID: CVCL_0152) cell lines were purchased from the ATCC in 2020. PC9 (RRID: CVCL_B260), A549 (RRID: CVCL_0023), MDA-MB-231 (RRID: CVCL_0062) cell lines were purchased from stem cell bank, Chinese Academy of Sciences (Shanghai, P.R. China) in 2018. BT-474 (RRID: CVCL_0179), SW837 (RRID: CVCL_1729), and JIMT-1 (RRID: CVCL_2077) cell lines were purchased from Pharma-Legacy in 2021. PC9GR cell line was generated by continuous gefitinib exposure of PC9 cells. All PDX models were obtained from Lidebiotech Co., Ltd. in 2021. Cells were maintained in RPMI1640 medium (SNU-16, COLO205, PC9, BT-474, COLO320DM, PC9GR, and AsPC-1) or DMEM (SW620, MDA-MB-231, SW837, and JIMT-1) or F-12K medium (A549) or McCoy's 5A medium (SK-BR-3) supplemented with 10% heat-inactivated FBS and cultured at 37°C and 5% CO_2 atmosphere. When cells were grown to approximately 80% confluence, they were dissociated from culture plates by treatment with 1× PBS and 1 mmol/L EDTA for 10 to 20 minutes.

All cell lines were authenticated by short tandem repeat analysis according to supplier information. All cells tested negative for *Mycoplasma* contamination with a Mycoplasma PCR Detection Kit (MP004, GeneCopoeia) prior to conducting cell-based assays. All cells and PDX models were used for the experiments within 5 to 15 passages and 2 to 5 passages, respectively after collection.

Immunofluorescence and flow cytometry

For cell surface proteins, immunofluorescence (IF) and flow cytometry assays were performed under nonpermeable conditions without detergent in the buffers. Antibody binding signal was detected using Alexa Fluor 488 and 594 goat anti-mouse IgG secondary antibodies (115-545-003 and 115-585-003, Jackson ImmunoResearch) or Flour 488 goat anti-human IgG secondary antibody (109-545-008, Jackson ImmunoResearch). Briefly, cells attached on coverslips (IF assays) or suspended in 1× PBS (Flow cytometry assays) were first fixed in 4% paraformaldehyde (PFA) for 10 minutes. PFA was then removed, and cells were rinsed three times with 1× PBS. Cells were blocked overnight at 4°C in a blocking buffer (1× PBS containing 10% normal goat serum). After removing the blocking buffer, cells were incubated with the primary antibody (dilution in the blocking buffer at 1:100 to 1,000 in accordance with each instruction) for 2 hours at room temperature. Cells were rinsed three times in 1× PBS before being incubated with fluorescence-labeled secondary antibody (diluted in blocking buffer at 1:500 dilution ratio with 1:10,000 Hoechst 33258; Sigma) for 1 hour. Finally, cells were rinsed three times with 1× PBS. IF images were recorded with OLYMBUS CKX53 fluorescence microscope. The three-dimensional reconstruction of the IF results was performed in ImageJ [National Center for Biotechnology Information, NIH (NCBI) free software]. The FACS data were collected with a BD Accuri C6 Plus system. A control sample without the primary antibody and another sample with isotype control antibody were used. The LIVE/DEAD Fixable Near-IR Dead Cell Stain Kit (L34960, Thermo Fisher Scientific) was used to exclude dead cells. Relative mean fluorescence intensity (rMFI) was calculated by the ratio of MFI of anti-target Ab-FITC/MFI of isotype control FITC.

Cytotoxicity and growth inhibition assay

Cells were seeded to a 96-well plate at an appropriate density depending on the cell line (typically 1,000–3,000 cells per well in a 100 μL of appropriate culture media). After overnight incubation, a concentration series of small molecule or naked antibodies or ADC drugs and controls were added. Cell viability was evaluated after 5 days. CCK-8 (10%, v/v, HY-K0301, MedChemExpress) or CellTiter Glo (CTG) buffer (G7570, Promega) was added into the wells, and incubation was continued for 1 to 2 hours at 37°C or 10 minutes, respectively. Absorbance values were measured on a Thermo Fisher Scientific Multiskan EX microplate reader using a wavelength of 450 nm for CCK-8 assay and luminescence detection for CTG assay. The IC_{50} values compared with untreated cells or treated with other controls were determined using inhibition dose–response curve fitting (GraphPad Prism 9).

Cell line and PDX studies

All tumor-bearing models were established in female BALB/c nude mice, which were purchased from Shanghai Family Planning Research Institute. All *in vivo* studies were performed in accordance with the local guidelines of the Institutional Animal Care and Use Committee of Multitude Therapeutics and with the approval of the committee. Briefly, 4 to 6 weeks old mice were housed together in sterilized cages and maintained under required pathogen-free conditions. Each cell suspension or tumor fragment was inoculated subcutaneously into female nude mice. When the tumor had grown to an appropriate volume, the tumor-bearing mice were randomized into treatment and control groups based on the tumor volumes, and dosing was started. Antibodies and ADCs were administered intravenously to the mice. Small-molecule drugs were administered orally. Tumor volume defined as 1/2 × length × $width^2$ was measured twice (3–4 days) a week. Tumor growth inhibition (TGI; %) was calculated as follows: TGI (%) = [1 – (mean of treatment group tumor volume on evaluation day)/(mean of control group tumor volume on evaluation day)] × 100. The mice were euthanized with CO_2 gas when they reached endpoints (tumor volume exceeding 3,000 mm^3, >10% reduction of body weight,

or clinical signs indicating that mice should be euthanized for ethical reasons).

Pharmacokinetics of AMT-562 in mice

Concentrations of ADC and total antibody quantity in plasma were determined with a validated ligand-binding assay; the lower limit of this quantitation was 0.02 μg/mL. Briefly, immune plates were coated with 1 μg/mL human HER3 protein, His Tag (ER3-H5223, ACROBiosystems Inc.) in coating buffer and kept overnight at 4°C. After washing, the plates were blocked and each serially diluted sample was added to the wells. After incubation for 1 to 2 hours at 37°C, the plates were washed and incubated with horseradish peroxidase (HRP)-conjugated anti-human IgG Fc secondary antibody (ab99759, Abcam Inc.) for total antibody measurement or a biotin-labeled anti-exatecan/DXd antibody (ADC-Ab0001, Abmart) for ADC measurement. After reaction at 37°C for 1 to 2 hours, 3,3′,5,5′-tetramethylbenzidine (TMB) solution (50-85-05, KPL Inc.) was added directly or after incubation with Streptavidin Protein, HRP (21124, Thermo Fisher Scientific Inc.) for 40–60 minutes at 37°C. A450 in each well was measured with a microplate reader. AMT-562 was intravenously administered at 10.0 mg/kg to mice. Plasma concentrations of ADC and total antibody were measured up to 21 days after dose.

ELISA

For a binding assay, immune plates were coated with 1 μg/mL Human His tag EGFR/HER2/HER3/HER4 protein, Cynomolgus His tag HER3 protein, and Mouse His tag HER3 protein that all purchased from ACROBiosystems in coating buffer and kept overnight at 4°C. After washing, the plates were blocked and each serially diluted substance was added to the wells. After incubation for 1 to 2 hours at 37°C, the plates were washed and incubated with HRP-conjugated anti-human IgG secondary antibody for 1 hour at 37°C. After washing, TMB solution was added and A 450 in each well was measured with a microplate reader.

Bioluminescence imaging analysis

Antibodies' affinity was measured with the bioluminescence imaging (BLI) system monitoring the interaction between molecules on Octet RED96e (ForteBio). AHC Biosensors were loaded with AMT-562 or patritumab. Binding measurement was performed in the absence or presence of NRG1 (13499-H08H, SinoBiological). NRG1 was used at 1:1 molar ratio with human HER3 protein. HER3 or the HER3-NRG1 complex were loaded to antibody-coated AHC Biosensors at serial diluted concentrations. The results were then analyzed with Octet RED96e software (ForteBio). K_D(M), K_{on}(1/Ms), and K_{dis}(1/s) were obtained after analysis.

Western blotting

Cells were treated with each substance and lysed with RIPA lysis buffer containing Halt Protease & Phosphatase Inhibitor Cocktail (78428, Thermo Fisher Scientific Inc.). The samples were loaded and separated by SDS-PAGE and blotted onto polyvinylidene difluoride membranes. The membranes were blocked and probed overnight with anti-phospho-HER3 antibody (#4791, Cell Signaling Technology), anti-HER3 antibody (#12708, Cell Signaling Technology), anti-phospho-AKT antibody (T40067, Abmart), anti-AKT antibody (T55561, Abmart), anti-phospho-ERK1/2 antibody (#4370, Cell Signaling Technology), anti-ERK1/2 antibody (#4695, Cell Signaling Technology), anti-β-tubulin antibody (R20005, Abmart) at 4°C. Then the membranes were washed and incubated with HRP-labeled secondary antibodies for 1 hour and visualized using the luminescent analyzer Tanon 4600 (Tanon, Inc).

IHC

The formalin-fixed, paraffin-embedded (FFPE) sections were generated from various cell lines, xenografted tissues. After deparaffinization and rehydration, sections were treated with antigen retrieval buffer (DAKO) and incubated with corresponding primary antibodies for 1 hour. Then the sections were washed and incubated with HRP-labeled secondary antibody (DAKO) for 1 hour. Target expression was then detected by using diaminobenzidine (DAB) staining buffer and hematoxylin (Harris). Histochemical scoring system (H-score) was used for target expression intensity evaluation. The expression grade was classified as 0 (H-score 0–14), 1+ (H-score 15–99), 2+ (H-score 100–199), and 3+ (H-score 299–300). Anti-HER3 IHC antibody (#12708) was purchased from Cell Signaling Technology.

Toxicity studies in monkeys

AMT-562 and Ab562-T1000-exatecan were intravenously administered intermittently at 3-week intervals over a 1-week period to cynomolgus monkeys. ADCs were given at 30 mg/kg on days 1, 22, and 43 for three times in total. Clinical signs, body weight, food consumption, and clinical pathology were monitored throughout the study. A necropsy was conducted the day after the last administration. The reversibility of the toxic changes was assessed in a subsequent 1-week recovery period in cynomolgus monkeys.

Organoids preparation and drug tests

Human colon cancer organoids were prepared by OneTar Biomedicine Co., Ltd. Organoids were harvested and seeded in 96-well cell culture plate (3799, Corning), when organoids grew to 50 μm in diameter. The sandwich method was used for drug tests. Before seeding, 50 μL 50% Matrigel (356231, Corning, Matrigel mixed with PBS 1:1) was dropped on the bottom of the culture plate as the bottom layer. Then 10 μL 10% Matrigel (Matrigel mixed with PBS 1:9) containing 50 ± 20 organoids was dropped on the bottom layer as the middle layer. A total of 200 μL organoids culture medium was added in each well as the upper layer. Drug tests started after a one-day culture. For drug tests, Calcein AM was used for living cell staining at day 0. The rectal cancer organoids (RCOs) culture medium was removed and replaced by 200 μL drug-containing culture medium. Then Calcein AM/propidium iodide (PI) was used for living/dead cell staining at day 6. EVOS M5000 was used for the photographing of organoids at day 0 and day 6. The size of living organoids was measured using ImageJ [National Center for Biotechnology Information, NIH (NCBI) free software].

Statistical analysis

All statistical analysis except for toxicity studies was performed using SAS System Release 9.1.3 and 9.2 (SAS Institute Inc.). Statistical analysis in toxicity studies was performed using MUSCOT (YukmsCo., Ltd.). All IC_{50} and ED_{50} values were determined by a Sigmoid Emax model, and dose dependency was evaluated by a Spearman rank correlation coefficient hypothesis test.

Statistics and data

Tests to determine significance are detailed in the relevant figure legends. Briefly, *t* tests or one-way ANOVAs were used to determine statistical significance of treatment conditions and two-way ANOVA to discriminate between the contributions of both dose and transformation.

Data availability

Correspondence and requests for data underlying the findings or materials should be addressed to Xun Meng (PhD): xun.meng@multitudetherapeutics.com.

Results

Ab562 binds to ECD1 of HER3 with a moderate binding affinity and is NRG1 independent

We decided to use a specific HER3-targeting antibody with a moderate binding affinity based on previous observations to minimize potential toxicity. A mouse mAb mAb562 was selected from a panel of hybridomas generated against HER3 extracellular domain or ECD (amino acids 20-643) and humanized IgG1 antibody Ab562 was derived from mAb562 subsequently. The binding epitope of Ab562 was mapped to ECD1 by domain swaps of mouse HER3 (Ab562 was not cross-reactive with mouse HER3; **Fig. 1A**). The binding affinity measured by ELISA of Ab562 on recombinant HER3 protein was 20–30 nmol/L, compared with about 3 nmol/L for patritumab (Supplementary Fig. S1A). In BLI measurement, the dynamic affinity was 15 nmol/L for Ab562 compared with about 3 nmol/L for patritumab (Supplementary Fig. S1B). Similar to patritumab, Ab562 bound to HER3 in the presence or absence of endogenous HER3 ligand NRG1, that is, to a more open (presence) or closed conformation (absence) of the ligand, in contrast with other HER3-binding antibodies (**Fig. 1B**; ref. 28). Despite its moderate affinity, Ab562 showed specific binding to HER3-overexpressing HEK293T cells but not wild-type cells (**Fig. 1C**) and specifically within the EGFR family (Supplementary Fig. S1C). Ab562 was cross-reactive to monkey (for toxicity evaluation) at a similar affinity but not to mouse HER3 ortholog like patritumab (Supplementary Fig. S1C and S1D).

Ab562 decreases cell surface HER3 expression modestly and is NRG1 independent

Because of internalization, HER3-targeting antibodies have been shown to variably decrease cell surface HER3 protein expression in the

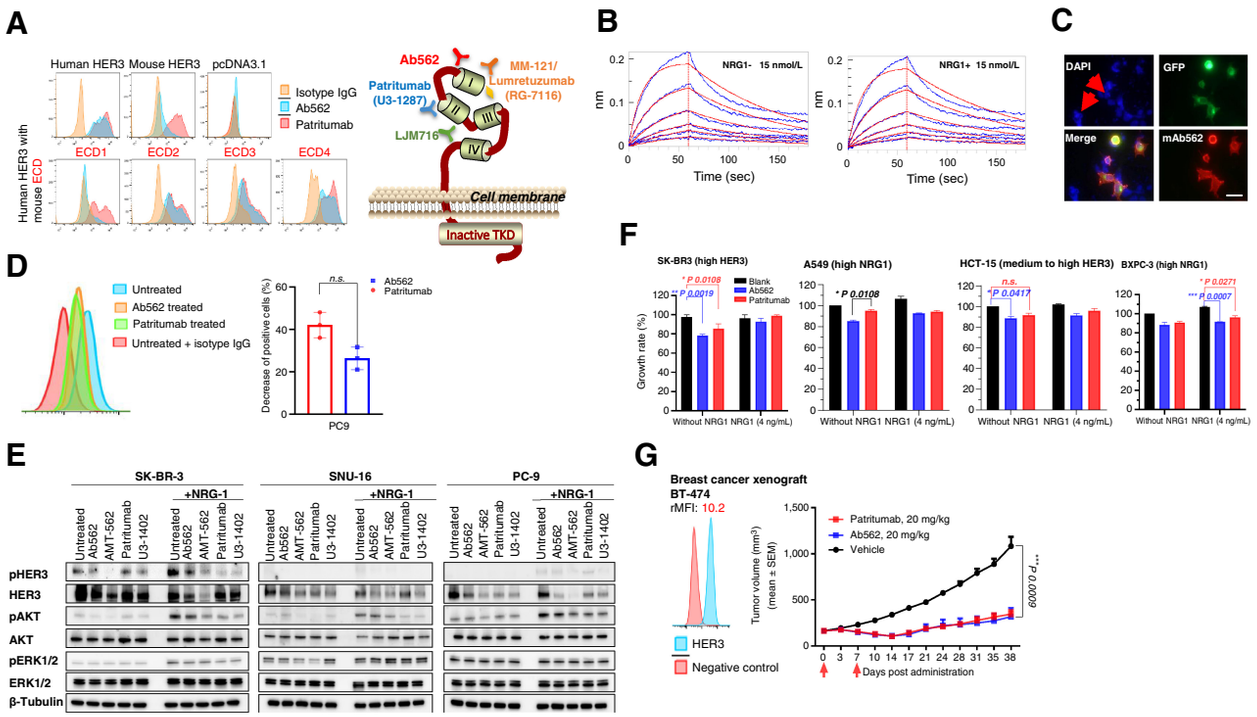

Figure 1.

Generation and characterization of Ab562, a novel HER3-targeting antibody. **A,** Ab562 binds to an epitope located in ECD1 determined by non–cross-reactive mouse HER3 domain swaps. Binding sites of other HER3-targeting mAbs: MM-121 or lumretuzumab (domain I) prevents NRG1 binding, LJM716 binds an epitope created by ECD domains II and IV in the HER3 closed conformation and patritumab binds the extracellular domain II. Modified from Kinisha Gala; Sarat Chandarlapaty. Molecular Pathways: HER3 Targeted Therapy. *Clin Cancer Res* 20, 1410–1416 (2014). **B,** Ab562 binding to HER3 in the absence (top) or presence (bottom) of NRG1 measured by BLI analysis. **C,** Target overexpression (colocalization of red mAb staining and green GFP-tagged target in 293T). Negative staining on the untransfected cells (blue only) is indicated by two red arrows. Scale bars, 10 μm. **D,** Ab562 caused less cell surface HER3 expression decrease in PC9 measured by flow cytometry. Change of HER3-positive cell percentage is tabulated on the right. Data shown are mean of triplicate measurements and error bars are SEM. Unpaired two-sided *t* test. *, $P < 0.05$; **, $P < 0.01$; ***, $P < 0.001$; ****, $P < 0.0001$. **E,** Effect of Ab562 on HER3 signaling. Western blot analysis for the phosphorylation of HER3, AKT, ERK1/2. Cells were incubated with 30 nmol/L patritumab or Ab562 with or without 1 ng/mL neuregulin-1 (NRG-1) for 1 hour. Western blot results from two ADCs, AMT-562 and P-GGFG-DXd, were also shown here (described in the section "*In vivo* functional validation of P-GGFG-DXd/U3-1402 and comparison with AMT-562"). **F,** *In vitro* proliferation experiments of Ab562 and patritumab. Cancer cell lines with HER3 and NRG1 expression data (labeled) treated with 100 μg/mL anti-HER3 antibodies for 5 days with cell viability determined by CTG assay. Cell proliferation values are relative to untreated cells and represent average of three replicates ± SEM. Unpaired two-sided *t* test. *, $P < 0.05$; **, $P < 0.01$. **G,** *In vivo* efficacy of Ab562 (blue) and patritumab in a breast cancer cell line xenograft model. High HER3 expression in BT-474 was shown as flow cytometry data on the left. Mice were intraperitoneally administered with antibodies (20 mg/kg) and on day 0 (tumor size reached an average of 150–200 mm^3) and subsequent dates indicated by red arrows. Each value represents the mean and SEM ($n = 5$). Unpaired two-sided *t* test. *, $P < 0.05$; **, $P < 0.01$; ***, $P < 0.001$.

absence or presence of endogenous HER3 ligand NRG1 (28–30). We examined the effect of Ab562 binding on cell surface HER3 expression. In PC9 with low endogenous NRG1 expression, Ab562 binding caused a 30% decrease of cell surface HER3 expression measured by flow cytometry, while patritumab caused an over 40% decrease (**Fig. 1D**; Supplementary Fig. S1E and S1F). In the presence of NRG1, both antibodies caused a further 50%–60% decrease in HER3 expression, with the addition of NRG1 leading to the biggest decrease (Supplementary Fig. S1E and S1G). In SNU-16, both Ab562 and patritumab caused a similar degree of decreased cell surface HER3 expression in both the absence and presence of NRG1, consistent with SNU-16's insensitivity to NRG1 (Supplementary Fig. S1H; ref. 30). Consistent with protein binding ELISA results, the binding of Ab562 was largely independent of NRG1 and led to decreased cell surface HER3 expression, although this decrease was smaller than the decrease caused by patritumab.

Ab562 inhibits HER3-mediated signaling

Ab562 was examined for inhibiting HER3-mediated signaling. Compared with the control (isotype control IgG antibody), Ab562 decreased the total quantity and phosphorylation of HER3 in multiple cancer cell lines (**Fig. 1E**). Adding NRG-1 induced increased phosphorylation of HER3, AKT, and ERK, while these phosphorylations were clearly inhibited by Ab562. In addition, the cells treated with Ab562 showed decreased total HER3 protein expression which is higher than patritumab (**Fig. 1E**). Patritumab showed similar inhibition in phosphorylation of HER3 (**Fig. 1E**).

Ab562 inhibits the proliferation of cancer cell lines *in vitro* and tumor growth *in vivo*

HER3-targeting antibodies have been shown to inhibit HER3-mediated cell growth and survival pathways (28–31). To this end, we measured the effect of Ab562 on the proliferation of a panel of cancer cell lines with a wide range of NRG1, HER2, HER3, and EGFR expressions, in the presence (4 ng/mL) or absence of NRG1 (Supplementary Fig. S1I). Ab562 inhibited cell growth in some but not all cell lines and showed better cell growth inhibition than patritumab in selective cells (**Fig. 1F**). Ab562 inhibited cell lines with either high HER3 expression (HCT-15 and SK-BR-3) or low HER3/high NRG1 expression (A549, BxPC-3; **Fig. 1F**). Overall Ab562 and patritumab showed significant but modest cell growth inhibition (10%–20%) in our experimental system compared with what was reported previously (30%–60%; refs. 28, 31).

To test the antitumor efficacy of Ab562 *in vivo*, we assayed TGI in a cell line-derived xenograft (CDX) model of breast cancer cell line BT-474 with high HER3 expression. Tumor-bearing mice were treated twice a week with vehicle control, 20 mg/kg of Ab562 or patritumab. Ab562 and patritumab showed significant and similar antitumor efficacy (**Fig. 1G**).

Design of AMT-562: balancing the efficacy and toxicity

HER3's low expression on cell surfaces poses a challenge for ADC targeting HER3. The number of HER3 molecules expressed on the surface of individual cells was measured by a QIFIKIT using murine form mAb562 in a panel of cancer cell lines representative of diverse solid tumors (**Fig. 2A**; Supplementary Fig. S2A and S2B). The average copy number/cell was 2,900 with a range of a few hundreds to >10,000. Compared with HER2, which shows an average of 120,000 copies/cell, HER3 showed significantly lower expression level (**Fig. 2A**), suggesting that an effective HER3 targeting would require a more potent payload. Exatecan was 10 times more potent than DXd in a panel of cancer cell lines with varying levels of HER3 expression (Supplementary Fig. S2C). To attach exatecan to Ab562, dipeptide Val-Ala (VA) linker and T moiety (hydrophilic modification of self-immolative pAB) were employed. Because of their effectiveness at attaching to exatecan, highly hydrophilic T1000 modified with a polysarcosine (pSAR) and moderately hydrophilic T800 modified with methylaminomethyl group were both tested (**Fig. 2B**; ref. 26). Ab562-VA-T800-exatecan (**AMT-562**) and Ab562-VA-T1000-exatecan (**AMT-562-T1000**) were readily generated with little aggregation, and both molecules were more hydrophilic than Ab562 conjugated to DXd through GGFG (Supplementary Fig. S2D). *In vivo* antitumor efficacy in the lung cancer cell line PC9 xenograft model showed that AMT-562 and AMT-562-T1000 were equally effective and outperformed P-GGFG-DXd (which was not effective; **Fig. 2C**), similar to previous results (15, 26).

T800- and T1000-based ADCs showed different pharmacokinetics in cynomolgus monkeys. For example, HER2-targeting MTX-1000 (Trastuzmab-T1000-exatecan) was more stable than MTX-800 (Trastuzmab-T800-exatecan) measured by half-life and exatecan release (Supplementary Fig. S3A and S3B). And these two ADCs displayed different toxicity profiles and both showed less clinical signs than reported for DS-8201a (Supplementary Fig. S3C). Similarly, AMT-562 and AMT-562-T1000 toxicity were compared in a pilot cynomolgus monkey (cross-reactive species) study. Body weight and hematologic parameters of both ADCs were largely within normal range (except for reticulocyte counts), although AMT-562-T1000 showed slightly larger changes than AMT-562 (Supplementary Fig. S4A–S4F). Serum chemistry of AMT-562 remained normal, as shown in the minimal changes in alanine aminotransferase and aspartate aminotransferase compared with AMT-562-T1000 (Supplementary Fig. S4G and S4H). Target organs of AMT-562 showed significantly less toxicity than those of AMT-562-T1000 although the highest non-severely toxic dose (HNSTD) for both molecules was 30 mg/kg (**Fig. 2D**; Supplementary Fig. S5A and S5B). Major toxicity findings for AMT-562 were mainly present in the gastrointestinal tract of monkeys, similar to other T moiety–exatecan ADCs (26). All findings were minimal or mild. Almost all treatment-related changes showed recovery or a trend of reversibility after a 1-week withdrawal period. AMT-562 showed comparable toxicity to U3-1402 (HNSTD of 30 mg/kg) although organs exhibiting toxicity were different (bone marrow versus skin; Supplementary Fig. S5C).

Similar to HER2-targeting ADC MTX-1000 and MTX-800, AMT-562 showed a different pharmacokinetic profile in monkeys than AMT-562-T1000. AMT-562 was less stable, with a shorter half-life and a faster and higher free payload release than AMT-562-T1000 (**Fig. 2E** and **F**; Supplementary Fig. S6A and S6B). Consequently, AMT-562 displayed a smaller AUC than AMT-562-T1000 (Supplementary Fig. S6C). AMT-562 stability was further evaluated in mice. After a single intravenous administration of AMT-562 at 10 mg/kg in normal mice, the pharmacokinetic profile of AMT-562 was similar to that of total Ab (Supplementary Fig. S6D and S6E). AMT-562 is stable with a half-life ($T_{1/2}$ 3.92 $\pm$ 1.3 days) comparable with the half-life of 4.52 $\pm$ 1.7 days for total antibody. The AUC of AMT-562 was almost 90% higher than that of a DXd-based ADC Ab562-GGFG-DXd, suggesting that T moiety–exatecan was significantly more stable than GGFG-DXd (Supplementary Fig. S6E), consistent with our data for other T moiety–exatecan ADCs (26). AMT-562 using T800 was selected to be the ADC of design based on its potent antitumor activity, lower toxicity, and favorable pharmacokinetic profile.

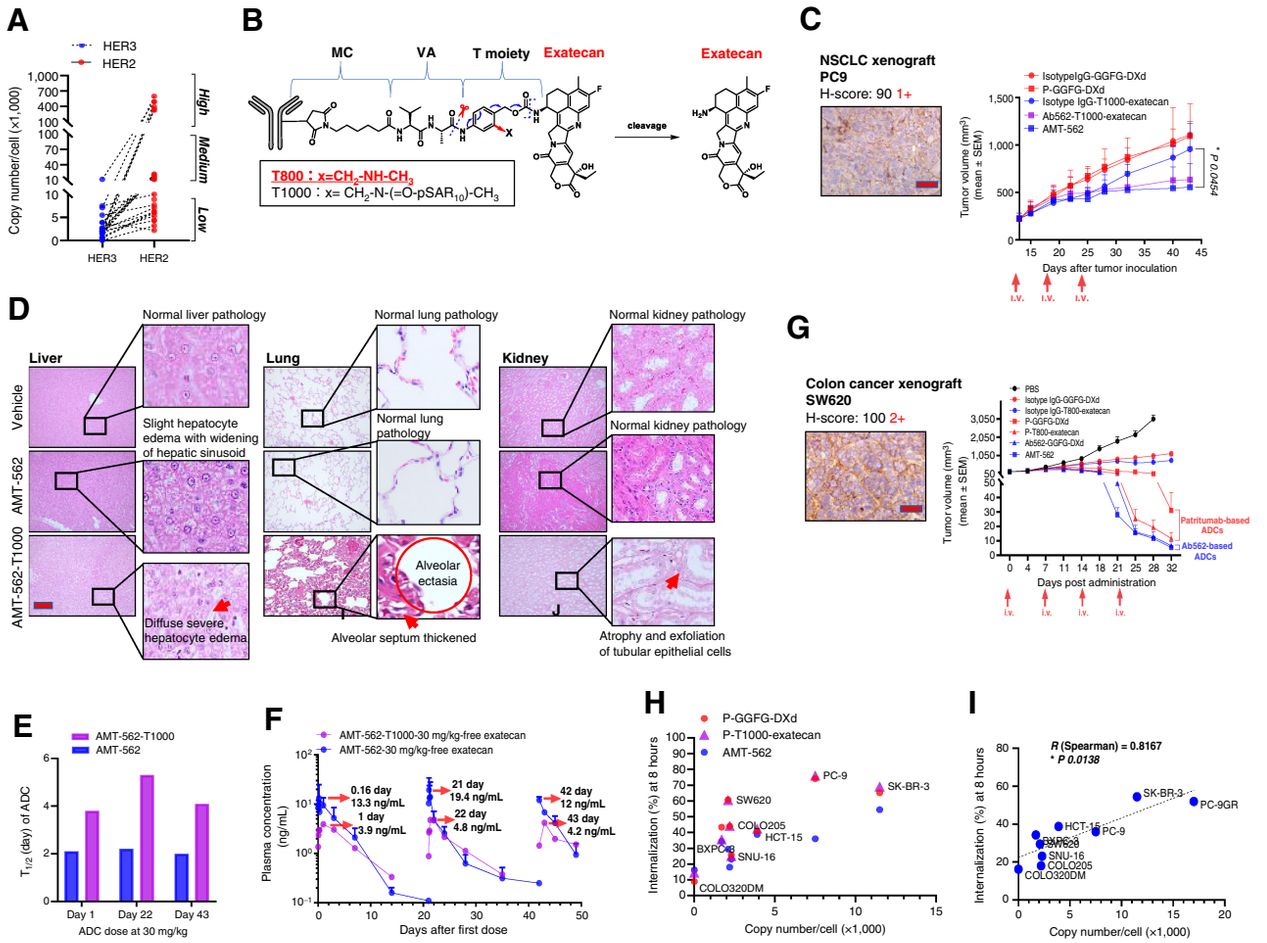

Figure 2.

Structure, stability, and cellular dynamics of AMT-562. **A,** HER3 and HER2 expression level on cancer cell surface measured by mAb562 and anti-HER2 mouse mAb (ab264541, Abcam). Expression was defined by number of HER3 and HER2 molecules per cell measured by flow cytometry (QIFIKIT). HER3 and HER2 expression on the same cell line was shown for comparison (connected by dotted lines). Expression level was classified as low, medium, and high by the number of target molecules per cell: 0–10,000 as low, 10,000–100,000 as medium, and 100,000–1 million as high. The average copy number of HER3 was 2,900 versus 120,000 for HER2. **B,** Structure of AMT-562. Exatecan was attached to T moiety, a hydrophilically modified self-immolative (indicated by a red scissor) pAB spacer. T moiety–exatecan was then linked to Ab562 through MC-VA linker. Exatecan is released as payload. T1000 with a pSAR or T800 with a methylaminomethyl group modification (rectangle box) was shown. **C,** *In vivo* efficacy of AMT-562, Ab562-T1000-exatecan, and P-GGFG-DXd in PC9 xenograft model. **D,** Representative hematoxylin and eosin staining of toxicity organs of AMT-562 and Ab562-T1000-exatecan. Scale bar, 200 μm. **E,** ADC half-life of AMT-562 and Ab562-T1000-exatecan from repeated dose toxicity studies in cynomolgus monkeys. **F,** Exatecan release of AMT-562 and Ab562-T1000-exatecan from repeated dose toxicity studies in cynomolgus monkeys. **G,** *In vivo* efficacy of orthogonal combinations of antibody and linker-payload pairs. ADCs were tested in an *in vivo* xenograft model of SW620. Four doses of 10 mg/kg ADCs were intravenously administered on day 0 (tumor size reached an average of 150–200 mm^3) and days indicated by red arrows. Each value represents the mean and SEM ($n = 5$). Unpaired two-sided *t* test. *, $P < 0.05$; **, $P < 0.01$; ***, $P < 0.001$. **H,** Internalization rate of AMT-562, P-GGFG-DXd, and P-T800-exatecan on cancer cell lines at 8 hours after ADC binding measured by flow cytometry. **I,** Correlation of exatecan release and target expression. HER3 expression on each cell line is determined by flow cytometry and exatecan concentration in the culture media at 24 hours after treatment with 100 nmol/L AMT-562 was determined by LC/MS-MS ($n = 3$).

In vivo functional validation of P-GGFG-DXd/U3-1402 and comparison with AMT-562

To compare antibody and ADC performance, four ADCs were prepared with an orthogonal combination of antibodies and linker-payload pairs (Supplementary Fig. S7A). The attachment of exatecan and DXd to both Ab562 and patritumab did not affect Ab562 or patritumab binding to HER3 protein by ELISA, yielding EC_{50} of 20–40 nmol/L for Ab562 and derived ADCs and 4–5 nmol/L for patritumab and derived ADCs, respectively (Supplementary Fig. S7B). The attachment of payloads to Ab562 or Patritumab did not affect antibody functionality, as shown in the similar effects of ADCs and antibodies in HER3 signaling (AMT-562 and U3–1402; **Fig. 1E**).

The equivalence in functionality between in-house prepared P-GGFG-DXd and reported U3-1402 was confirmed by their similar *in vivo* tumor inhibition potency on day 31 in colon cancer cell line SW620 xenograft model (15). Two ADCs derived from Ab562, AMT-562, and Ab562-GGFG-DXd, showed higher antitumor efficacy than their counterpart ADCs derived from Patritumab (P-T800-exatecan and U3-1402/P-GGFG-DXd), highlighting the superiority of Ab562 over patritumab for ADC development (**Fig. 2G**;

Supplementary Fig. S7C). On day 46, AMT-562 produced 4 complete responses (CR) out of 5 mice comparing with 1 out of 5 for P-GGFG-DXd (Supplementary Fig. S7D). Across all experimental groups, the mice showed no abnormalities in general condition, nor did they exhibit change in body weight (not data shown) for all tested ADCs. In another HER3-low expression and Herceptin-resistant model of JIMT-1, AMT-562 showed significant antitumor efficacy, but the tumor was resistant to P-GGFG-DXd (Supplementary Fig. S7E), consistent with a previous report of U3-1402's ineffectiveness in this model (16). Ultimately, P-GGFG-DXd was confirmed to be functionally equivalent to reported U3-1402 and Ab562 and T800-exatecan were shown to be superior to patritumab and GGFG-DXd, respectively.

Internalization and intracellular trafficking of AMT-562 in cancer cells

AMT-562's binding and internalization as well as exatecan release were evaluated in cancer cell lines. AMT-562 internalized efficiently with a $T_{1/2}$ of 0.5–2 hours in different cell lines and there was a proportional relationship between HER3 expression level and internalization rate (**Fig. 2H**; Supplementary Fig. S7F). AMT-562 internalized less efficiently than P-GGFG-DXd in most of cell lines, showing that naked antibody binding had consistent effects on cell surface HER3 expression (Ab562 causing a smaller decrease in cell surface HER3 expression; **Fig. 2H**). Attaching DXd or exatecan to patritumab (P-GGFG-DXd vs. Patritumab-T800-exatecan) led to the same internalization rate, suggesting payload had minimal effect on ADC internalization (**Fig. 2H**). The exatecan quantity released into the culture media 24 hours after the AMT-562 binding and internalization into the cells correlated with the cell surface HER3 expression level of each cell line (**Fig. 2I**).

In vitro cytotoxicity and bystander killing of AMT-562

Consistent with the payload cytotoxicity levels, AMT-562 showed more potent *in vitro* cytotoxicity activity than P-GGFG-DXd in HER3-expressing cancer cell lines, particularly in cells with low level of HER3 expression (Supplementary Fig. S8A–S8D). Naked antibodies patritumab and Ab562 and isotype control ADCs did not show measurable activities (Supplementary Fig. S8B–S8D). Both ADCs did not show activity in HER3-negative cell lines MDA-MB-231, suggesting that ADC cytotoxicity was mediated by the binding of antibodies to HER3 on the cell surface (Supplementary Fig. S8D).

We have shown that T moiety-exatecan–based HER2-targeting ADC MTX-1000 (Trastuzmab-T1000-exatecan) showed a higher bystander killing efficacy than its DXd counterpart ADC T-GGFG-DXd/DS-8201a (26). AMT-562's bystander killing efficacy was measured using an *in vitro* culture system with single or cocultures of $HER3^-$ (COLO320DM) and $HER3^+$ (PC9GR) cell lines (**Fig. 3A**; Supplementary Fig. S8E and S8F). After 5 days of incubation, cells were sorted for HER3 expression by flow cytometry (Supplementary Fig. S8E). AMT-562 killed HER3-COLO320DM cells efficiently (**Fig. 3A**; Supplementary Fig. S8E). Negative control ADCs did not induce cell killing compared with untreated wells, confirming the bystander killing effect of AMT-562. In comparison, P-GGFG-DXd showed less cytotoxicity and bystander killing was not significant versus isotype ADC control (**Fig. 3A**).

Pharmacodynamic response of AMT-562: intratumoral and in patient-derived organoids

Pharmacodynamic response measured by DNA-damaging marker γH2A.X and apoptosis marker Cleaved Caspase-3 were used to probe the mechanism of AMT-562 *in vivo*. A single dose of 10 mg/kg of AMT-562 was administrated to colon cancer xenograft COLO205 and tumor growth was observed for 21 days (**Fig. 3B**). Pharmacodynamic response of AMT-562's DNA-damaging was rapid starting at the 4-hour mark and continuing (**Fig. 3C**). Both AMT-562 and P-GGFG-DXd produced significant DNA damaging compared with the vehicle control but the AMT-562 signal showed up earlier, was higher and more persistent (**Fig. 3C** and **D**). Similar results were observed for apoptosis with AMT-562 resulted in significant cell death starting from 48 hours after drug administration (**Fig. 3E** and **F**).

To gain cellular resolution of ADC potency and payload distribution, tumor penetration of AMT-562 and P-GGFG-DXd was evaluated by cell imaging and HER3-positive patient-derived colon cancer organoids (PDO; refs. 26, 32; Supplementary Fig. S9A). In two PDOs, AMT-562 caused more cell death to prevent organoid growth than P-GGFG-DXd (**Fig. 3G–I**; Supplementary Fig. S9B and S9C). Notably, the cell death signals (PI staining) for AMT-562 were more widespread and deeper inside the organoid compared with more peripheral and less staining for P-GGFG-DXd (**Fig. 3G**). Both PDOs grew normally without ADC treatment (Supplementary Fig. S9D).

HER3 expression in digestive system tumors

To evaluate antitumor activity of AMT-562 in tumors derived from digestive organs including the esophagus, pancreas, stomach, colon, and rectum, we first assayed HER3 expression in a panel of PDX models with IHC (Supplementary Fig. S10A). HER3 expression ranged from 40% to 60% in these tumors (Supplementary Fig. S10B). Even HER3 was only positive in about 40% of colon cancer samples, most of which were medium and strong expression (Supplementary Fig. S10C). HER3 expression in rectal cancer was higher, at 70% (Supplementary Fig. S10C). HER3 was expressed in most cases of esophagus adenocarcinoma (67%) but only in 20% of esophagus squamous cell carcinoma, and expression level was low for both subtypes at IHC 1+ (Supplementary Fig. S10D). HER3 showed strong expression in about 50% of pancreatic cancer samples. On the basis of the expression data, we comprehensively tested AMT-562 antitumor efficacy in xenograft (CDX)/PDX models representing digestive system cancers and compared AMT-562 performance with P-GGFG-DXd (**Figs. 4** and **5**; Supplementary Fig. S11A–S11F). Notably, U3-1402 efficacy has only been reported in breast and lung cancer despite a broad overexpression profile of HER3 in solid tumors (Supplementary Fig. S10E).

AMT-562 antitumor efficacy in pancreatic, esophagus, and gastric cancer

AMT-562 antitumor efficacy was evaluated in four pancreatic models *in vivo* (**Fig. 4A**). In the pancreatic cancer cell line BxPC-3 model with a BRAF inhibitor–resistant deletion (33), AMT-562 showed significant tumor inhibition but P-GGFG-DXd did not (Supplementary Fig. S11A). In AsPC-1, AMT-562 showed more potent tumor inhibition than P-GGFG-DXd at 5 mg/kg and 10 mg/kg, respectively (**Fig. 4B**). In a pancreatic cancer PDX model with *KRAS* G12R and G34C double mutation, AMT-562 produced a CR in 3 out of 5 mice. P-GGFG-DXd also showed strong tumor inhibition but not a CR (**Fig. 4C**). Similarly, AMT-562 caused significant TGI in a low-HER3 expression pancreatic PDX model while P-GGFG-DXd did not (**Fig. 4D**). In esophagus PDX models with low HER3 expression (**Fig. 4E**), AMT-562 outperformed P-GGFG-DXd (**Fig. 4F–H**).

HER3 was overexpressed in about 50% of gastric cancer cases with low to moderate expression (Supplementary Fig. S10B). AMT-562's *in vivo* antitumor activity was assessed in multiple xenograft CDX and

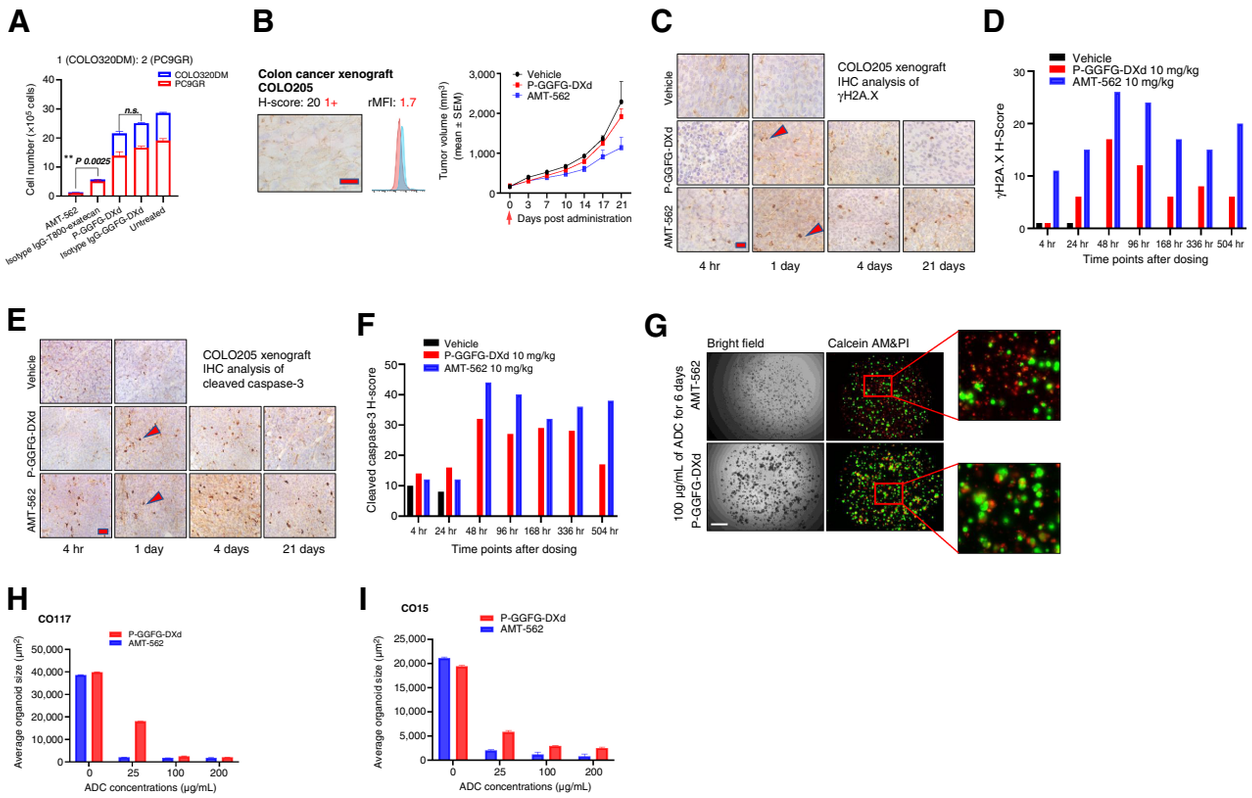

Figure 3.

Pharmacodynamics of AMT-562 *in vivo* and in organoids. **A,** Bystander killing effect of AMT-562 and P-GGFG-DXd in coculture conditions *in vitro*. PC9GR and COLO320DM cells were cocultured and treated with 50 nmol/L ADCs for 5 days. After collecting adherent cells, cell number and ratio of HER3-positive and HER3-negative cells were determined by a cell counter and a flow cytometer, respectively. Each bar represents the mean and SD ($n = 3$). **B,** *In vivo* efficacy of AMT-562 and P-GGFG-DXd in COLO205 xenograft model. CDX mice were intravenously administered with indicated ADCs and vehicle control (10 mg/kg) on day 0 (tumor size reached an average of 150–200 mm^3) indicated by red arrows. Each value represents the mean and SEM ($n = 2$). **C** and **D,** γH2AX foci induction in the HER3+ COLO205 tumor model by IHC analysis. Tumors were collected at the indicated timepoints and FFPE for IHC analysis. γH2AX IHC antibody (#9718, Cell Signaling Technology) was used for detection. Representative images were shown for indicated days. Positive γH2AX foci (black spots) were indicated by red arrows. Scale bar, 20 μm (**C**). Time course of γH2AX H-score. Each value represented the mean (2 mice, two measurements each; **D**). **E** and **F,** Cell death induction in COLO205 xenograft model by IHC analysis of Cleaved Caspase-3. Cleaved Caspase-3 IHC antibody (#9579, Cell Signaling Technology) was used for detection. Representative images were shown for indicated days. Positive signals (black spots) were indicated by red arrows. Scale bar, 20 μm (**E**). Time course of Cleaved Caspase-3 H-score. Each value represented the mean (2 mice, two measurements each; **F**). **G,** Colon cancer PDOs (CO117&CO15) response to AMT-562 and P-GGFG-DXd. Representative images of brightfield (left) and live/dead cells (right) for CO117 was shown. Colon cancer PDOs were treated with AMT-562 or P-GGFG-DXd at a serial concentration for 6 days. Live cells were stained by Calcein AM (green) and dead cells by PI (red). Scale bar, 200 μm. **H** and **I,** Organoid size at day 0 and day 6 of ADCs treatment. Surviving organoid size was measured. Data shown are means ± SEM from two independent measurements.

PDX models (Supplementary Fig. S11B). In the HER3 low expression SNU-16 gastric cancer xenograft model measured by flow cytometry and IHC, tumors were resistant to P-GGFG-DXd (no tumor inhibition after three 10 mg/kg consecutive weekly dosing). In contrast, AMT-562 inhibited tumor growth significantly at both 10 mg/kg (TGI 90%) and 5 mg/kg (TGI 60%) dosing (Supplementary Fig. S11C). In other gastric cancer models, AMT-562 was either significantly better than or similarly effective as P-GGFG-DXd (**Fig. 4H**; Supplementary Fig. S11D–S11F). Together, AMT-562 outperformed U3-1402 for tumor inhibition in pancreatic, esophagus, and gastric cancer models (**Fig. 4I**).

Antitumor activity of AMT-562 in colorectal cancer

HER3 was overexpressed in about 40% and 70% of colon and rectal cancer, respectively, and with more tumors exhibiting medium and higher expression (Supplementary Fig. S10C). AMT-562 was evaluated in colorectal cancer models representative of unmet need characterized by microsatellite stable (MSS), *TP53*, and *KRAS* mutation. In the (MSS) COLO205 xenograft model with $BRAF^{V600E}$ mutation, AMT-562 showed significantly better TGI than P-GGFG-DXd (Supplementary Fig. S12A). PDX-361795 was derived from a colon cancer with liver metastasis and *KRAS-TP53* double mutation. AMT-562 induced tumor regression while P-GGFG-DXd was ineffective (**Fig. 5A**). AMT-562 also showed significantly better TGI than P-GGFG-DXd in another colon cancer PDX (**Fig. 5B**). However, in a rectal cancer PDX, both AMT-562 and P-GGFG-DXd were similarly effective (**Fig. 5C**). On the other hand, in a rectal cancer model with a relatively high HER3 expression (H-score 200, 3+), AMT-562 showed significant tumor inhibition, although at a lesser degree than in other models (**Fig. 5D**). Ultimately, AMT-562 has shown high-quality antitumor efficacy in digestive system tumors, even in low HER3 expression or tumors with challenging genetic profiles. In all diversely representative colon cancer models, AMT-562 outperformed DXd and patritumab-based ADC (**Fig. 5E** and **F**).

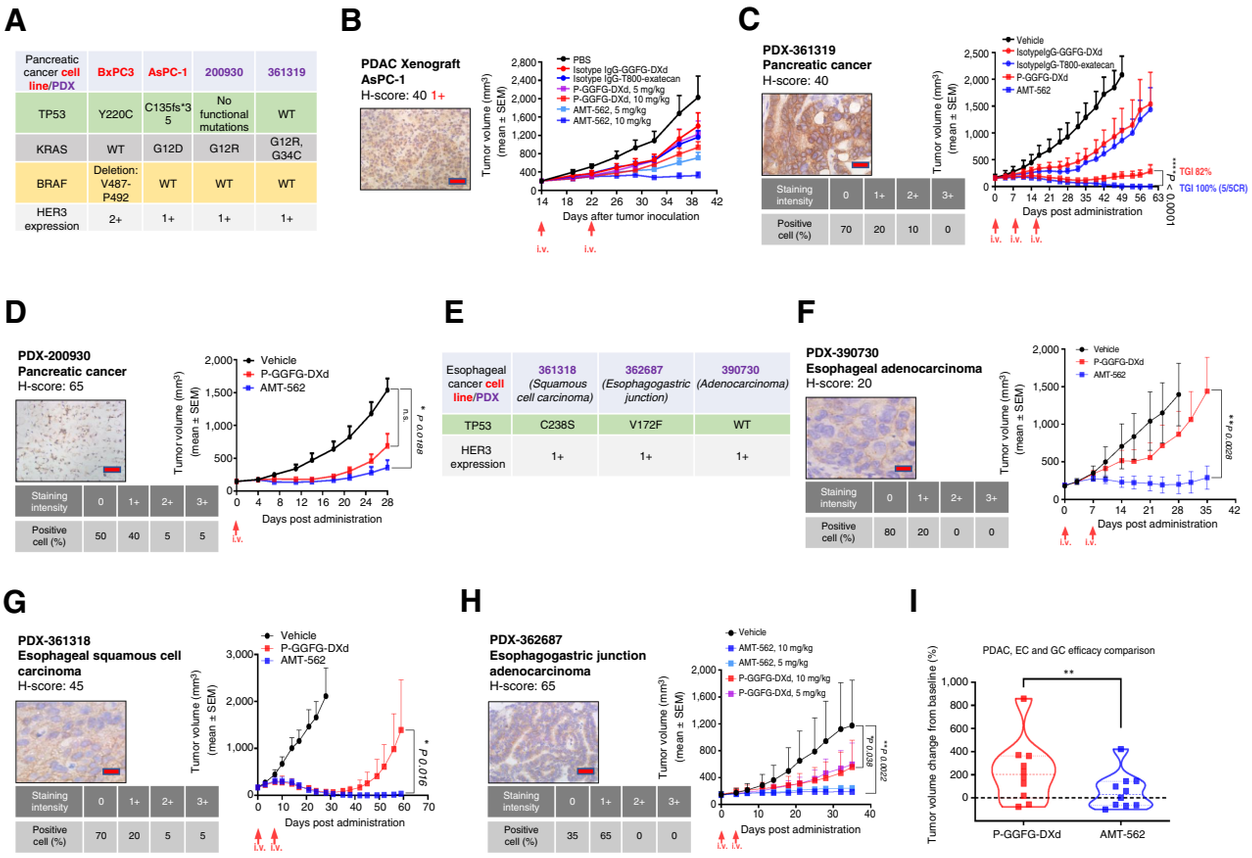

Pancreatic cancer cell line/PDX	BxPC3	AsPC-1	200930	361319
TP53	Y220C	C135fs*35	No functional mutations	WT
KRAS	WT	G12D	G12R	G12R, G34C
BRAF	Deletion: V487-P492	WT	WT	WT
HER3 expression	2+	1+	1+	1+

Staining intensity	0	1+	2+	3+
Positive cell (%)	70	20	10	0

Staining intensity	0	1+	2+	3+
Positive cell (%)	50	40	5	5

Staining intensity	0	1+	2+	3+
Positive cell (%)	80	20	0	0

Esophageal cancer cell line/PDX	361318 (Squamous cell carcinoma)	362687 (Esophagogastric junction)	390730 (Adenocarcinoma)
TP53	C238S	V172F	WT
HER3 expression	1+	1+	1+

Staining intensity	0	1+	2+	3+
Positive cell (%)	70	20	5	5

Staining intensity	0	1+	2+	3+
Positive cell (%)	35	65	0	0

Figure 4.

In vivo antitumor efficacy of AMT-562 in pancreatic, esophagus and gastric cancer. **A–E,** Information of CDX/PDX models of pancreatic (**A**) or esophagus (**E**) cancer. Shown is mutation status of *TP53/KRAS/BRAF*. HER3 expression level is indicated on the basis of IHC score or flow cytometry. Subtype of esophagus cancer was indicated. **B–D,** *In vivo* efficacy of AMT-562 and P-GGFG-DXd and control ADCs in pancreatic cancer models. **F–H,** *In vivo* efficacy of AMT-562 and P-GGFG-DXd and control ADCs in esophagus cancer models. For all *in vivo* models, target and cell line/PDX tumor type is labeled. Target expression in each model is shown as flow cytometry (rMFI) and/or IHC image on untreated mouse tumor tissue and H-score. Scale bars, 20 μm. CDX/PDX mice were intravenously administered with indicated ADCs (10 mg/kg unless otherwise labeled) and on day 0 (tumor size reached an average of 150–200 mm^3) and subsequent dates indicated by red arrows. Each value represents the mean and SEM ($n = 4$ or 5). Unpaired two-sided *t* test. *, $P < 0.05$; **, $P < 0.01$; ***, $P < 0.001$. **I,** A summary of tumor volume change of AMT-562 versus P-GGFG-DXd in pancreatic, esophagus, and gastric cancer models.

AMT-562 synergizes with inhibitor of CHEK1 and therapeutic antibodies in colorectal cancer cells

Bevacizumab-targeting VEGF and cetuximab-targeting EGFR are approved therapeutic antibodies, both as single agent or in combination, for colorectal cancer (34). AMT-562 in combination with bevacizumab or cetuximab was tested in a colon cancer model after AMT-562 alone was less effective (**Fig. 5G**). AMT-562 in combination with bevacizumab or cetuximab produced significantly better antitumor activity than AMT-562 or bevacizumab/cetuximab alone (**Fig. 5G** and **H**). P-GGFGF-DXd also exhibited synergy with bevacizumab/cetuximab, but to a lesser degree.

In colon cancer cells, Top I inhibitors such as SN-38 or exatecan were shown to be synergistic with DNA-damaging pathway mediator inhibitors targeting PARP, ATR, or CHEK1 inhibitors (26, 35). Both exatecan and DXd showed synergistic cytotoxicity in combination with Rabusertib (CHEK1 inhibitor) in the SW837 cell line (with *TP53* R248W and *KRAS* G12C mutation; medium HER3 expression with a rMFI of 3.4; Supplementary Fig. S12B). AMT-562 showed higher synergy with Rabusertib than P-GGFG-DXd (Supplementary Fig. S12C and S12D). *In vivo*, AMT-562 showed significant synergy with Rabusertib in COLO205 (Supplementary Fig. S12E). The combination treatment of ADCs and Rabusertib was tested in a rectal cancer PDX model in which both AMT-562 and P-GGFG-DXd showed initial efficacy but tumors regrew. The combination of AMT-562 and Rabusertib produced long-lasting antitumor efficacy with 3 of 5 CRs (**Fig. 5I**). P-GGFG-DXd in combination with Rabusertib also showed significantly better results than P-GGFG-DXd alone. However, AMT-562 alone was equivalent to P-GGFG-DXd in combination with Rabusertib, suggesting an overall higher synergy of AMT-562 with CHEK1 inhibition.

AMT-562 shows efficacy in EGFR-mutant, TKI-resistant, and wild-type NSCLC

We surveyed HER3 expression in a panel of NSCLC PDX samples by IHC. HER3 expression was positive in about 70% of adenocarcinoma and 40% of squamous cell carcinoma (no expression in small cell lung cancer; Supplementary Fig. S13A and S13B). In NSCLC, the percentage of overexpression (77%) in EGFR-mutated (EGFRm) was higher than in that wild-type (65%). Particularly, high HER3 expression (IHC 3+) was 14% in EGFRm samples versus 6% in wild-type

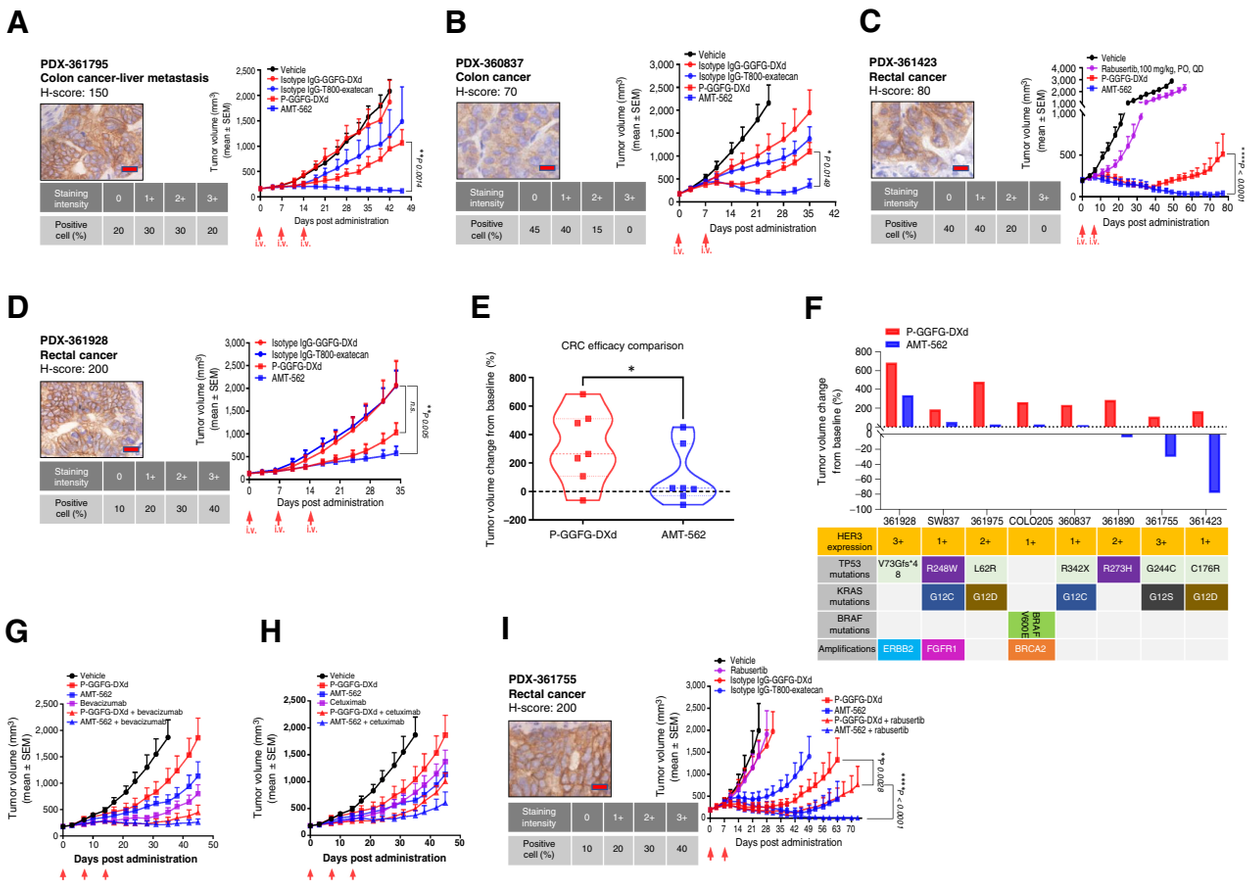

Figure 5.

AMT-562 is more effective as single agent or in combination therapy for colorectal cancer. **A–D,** Single ADC agent efficacy in PDX models. A PDX with liver metastasis of a relatively high HER3 expression (**A**). A low HER3 expression PDX (**B**). A tumor resistant to Rabusertib (CHEK1 inhibitor; **C**). A high HER3 expression PDX (**D**). A summary of tumor volume change of AMT-562 versus P-GGFG-DXd in colorectal cancer models (**E**) and information of CDX/PDX models of colorectal cancer (**F**). Shown is mutation status of *TP53/KRAS/BRAF* and other amplifications. HER3 expression level is indicated on the basis of IHC score. **G–I,** Combination therapy of ADC with VEGF/EGFR/CHEK1 inhibitor, respectively. *In vivo* efficacy of single-agent AMT-562, P-GGFG-DXd and control ADCs or in combination treatment of colon cancer models. Target and cell line/PDX tumor type is labeled. Target expression in each model is shown as flow cytometry (rMFI) and/or IHC image on untreated mouse tumor tissue and H-score. Scale bars, 20 μm. CDX/PDX mice were intravenously administered with indicated ADCs (10 mg/kg unless otherwise labeled) and on day 0 (tumor size reached an average of 150–200 mm^3) and subsequent dates indicated by red arrows. Each value represents the mean and SEM ($n = 4$ or 5). Unpaired two-sided *t* test. *, $P < 0.05$; **, $P < 0.01$; ***, $P < 0.001$. For combination treatments, bevacizumab was dosed at 5 mg/kg, i.p., once a week for 3 weeks. Cetuximab was dosed at 1 mg/animal, i.p., once a week for 3 weeks. Rabusertib was dosed at 100 mg/kg, orally, every day for 21 days.

(Supplementary Fig. S13C), consistent with an elevated HER3 expression in EGFRm that was reportedly previously. In the clinic, U3-1402/P-GGFG-DXd has reported efficacy in EGFR-mutant, TKI-resistant, and EGFR wild-type tumors, although the response was higher in EGFR-mutant, TKI-resistant tumors due to elevated HER3 expression (Supplementary Fig. S13D; refs. 18, 19).

AMT-562 was evaluated in a panel of clinically-relevant NSCLC PDX models representative of resistance mechanisms. In a series of low HER3 expression (IHC 1+) NSCLC with different mutations and TKI-resistant mechanisms, AMT-562 produced tumor regression, including CRs, and was significantly more potent than P-GGFG-DXd (**Fig. 6A–C**). One of models was derived from a patient with *EGFR ex19del*/C797S/T790M-activating mutation that lacks approved therapeutic options (**Fig. 6C**). In this model, AMT-562 significantly outperformed the suggested brigatinib combined with cetuximab to inhibit tumor growth (36). In a model with moderate HER3 expression (2+) and *EGFR ex19del*/*MET* Amplification resistant to third-generation TKI, both AMT-562 and P-GGFG-DXd showed potent antitumor efficacy (**Fig. 6D**). However, P-GGFG-DXd group showed a shorter response duration as tumors started to regrow after 3 weeks of drug dosing, eventually leading to significant antitumor efficacy difference between P-GGFG-DXd and AMT-562. Finally, in a PDX (wild-type EGFR) with a ROS1 translocation resistant to ALK TKI Crozitinib (37), both AMT-562 and P-GGFG-DXd produced tumor regression with a single dose of ADCs (**Fig. 6E**). Together, our data demonstrated that AMT-562 overcame different resistance mechanisms of EGFR mutation and often outperformed P-GGFG-DXd (**Fig. 6F**; Supplementary Fig. S13E–S13G).

Combination therapy of AMT-562 with EGFR TKI or *KRAS* G12C inhibitor in lung cancer

The usage of EGFR TKI was shown to increase HER3 expression and therefore boost the antitumor efficacy of HER3-targeting ADC P-GGFG-DXd (38, 39). A gefitinib resistant version (PC9GR) of

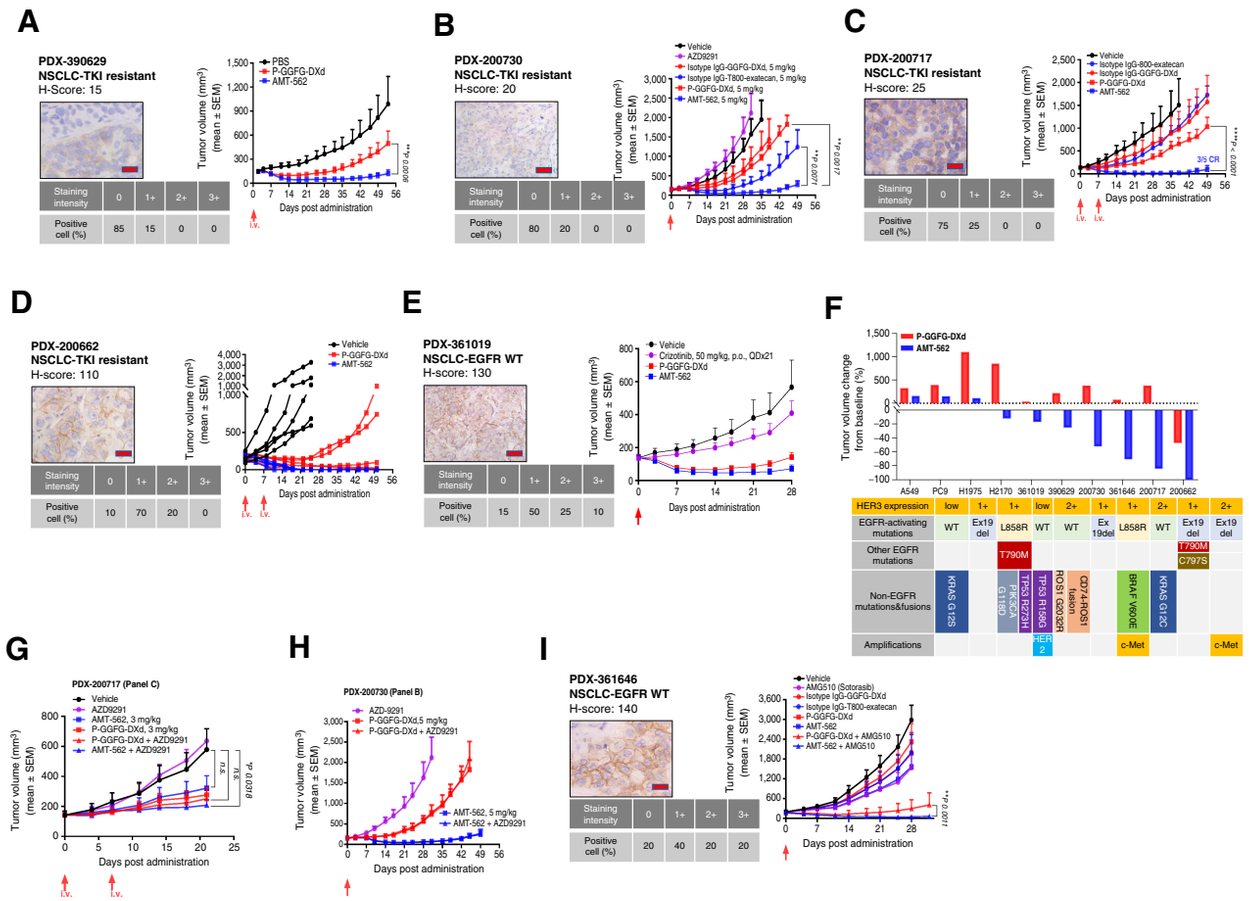

Figure 6.

AMT-562 targets lung cancer resistance alone or in combination therapy. **A–E,** Single ADC agent efficacy in PDX models. PDXs resistant to third-generation EGFR TKI AZD9291(**A–D**). PDX with EGFR WT genotype (**E**). **F,** Information of CDX/PDX models of NSCLC and tumor volume change of AMT-562 versus P-GGFG-DXd in NSCLC models. Shown is mutation status of EGFR, other mutations/amplifications. HER3 expression level is indicated on the basis of IHC score or flow cytometry. **G,** Combination treatment of lowered dose of ADCs and EGFR TKI AZD9291. The efficacy of 10 mg/kg of ADCs in this model was shown in **C**. **H,** Combination treatment of ADCs and AZD9291 in an AMT-562–sensitive but P-GGFG-DXd–resistant PDX model. See **B**. **I,** *In vivo* efficacy of HER3-targeting ADCs alone or in combination with *KRAS* G12C inhibitor AMG510 (Sotorasib) in a NSCLC PDX with *KRAS* G12C mutation. Target and cell line/PDX tumor type is labeled. Target expression in each model is shown as flow cytometry (rMFI), gene expression copy number and/or IHC image on untreated mouse tumor tissue and H-score. Scale bars, 20 μm. CDX/PDX mice were intravenously administered with indicated ADCs (10 mg/kg unless otherwise labeled) or other drugs (dose indicated) on day 0 (tumor size reached to an average of 150–200 mm^3) and subsequent dates indicated by red arrows. Each value represents the mean and SEM ($n = 4$ or 5). Unpaired two-sided *t* test. *, $P < 0.05$; **, $P < 0.01$; ***, $P < 0.001$. For combination treatments, AZD9291 was dosed at 10 mg/kg, orally, every day for 21 days. AMG510 was dosed at 30 mg/kg, orally, every day for 21 days.

NSCLC cell line PC9 was generated by continuous gefitinib exposure of PC9 cells (Supplementary Fig. S14A). Cell surface expression of HER3 in PC9GR (gefitinib resistant) showed a 2- to 3-fold increase in PC9, measured by flow cytometry (Supplementary Fig. S14B), which is consistent with a previous report (13). Exatecan/DXd showed a slight (1.5- to 2-fold) decrease in cytotoxicity toward PC9GR than PC9, with exatecan still remaining 10 times more potent than DXd (IC_{50} of 5.2 nmol/L vs. 48 nmol/L; Supplementary Fig. S14C). Interestingly, while AMT-562 showed similar cytotoxicity in PC9 and PC9GR (IC_{50} of 30 nmol/L vs. 47 nmol/L), P-GGFG-DXd showed a significant decrease in cytotoxicity (almost five times less) toward PC9GR (IC_{50} of 440 nmol/L) than PC9 (IC_{50} of 90 nmol/L), suggesting that P-GGFG-DXd may be much less effective in TKI-sensitive and -resistant cells (Supplementary Fig. S14D), even TKI-resistant cells with higher HER3 expression. Indeed, P-GGFG-DXd was resistant to PC9 *in vivo* while AMT-562 showed significant antitumor efficacy in the same model (**Fig. 2C**). A combination of ADCs and gefitinib dramatically increased ADC cytotoxicity while naked antibodies and Isotype IgG ADCs were not effective (Supplementary Fig. S14D), pointing to a combination strategy for more effective therapy.

Combination therapy was tested in NSCLC PDX models. Only AMT-562 (at a reduced dose) showed synergy with EGFR TKI inhibitor AZD9291 in a TKI-resistant model (**Fig. 6G**). HER3 expression increased due to AZD9291 usage but was reduced by AMT-562 due to cell surface antigen consumption, and the combined use of AMT-562 and AZD9291 induced a higher HER3 expression than AMT-562 alone (Supplementary Fig. S14E). P-GGFG-DXd was not synergistic with AZD9291 in a TKI-resistant model (AMT-562 alone was already highly effective in this model; **Fig. 6H**). Finally, in an EGFR wild-type NSCLC with a *KRAS* G12C mutation, single

agent ADC or *KRAS* G12C inhibitor Sotorasib (AMG510) was not effective. However, a combination treatment of AMT-562 with Sotorasib produced highly synergistic antitumor efficacy (**Fig. 6I**), outperforming the combined use of P-GGFG-DXd and Sotorasib. The PDX result was consistent with the results shown by *in vitro* payload or ADC combined with the *KRAS* G12C inhibitor (Supplementary Fig. S14F–S14H).

Discussion

A HER3-targeting ADC with an improved therapeutic index is expected to increase response rate in tumors against which HER3-ADC is effective, such as NSCLC or breast cancer, and elicit meaningful clinical responses from more HER3-positive tumor types. AMT-562 is a novel T moiety-exatecan–based HER3-targeting ADC designed with this goal in mind. Compared with DXd and SN-38, exatecan has a more favorable payload profile characterized by higher potency, lower sensitivity to MDR, higher cell permeability, and a known toxicity profile that has been clinically tested. T moiety was proven to provide better hydrophobic payload masking, generating more stable ADC and circumventing structural change in clinically-tested exatecan and linker structures (26). To pair with T moiety–exatecan for HER3 targeting, we used a novel antibody with high specificity, high hydrophilicity, and moderate affinity. The resulting AMT-562 translated the superior pharmacologic features of exatecan into an improved antitumor performance and a favorable pharmacokinetic and toxicity profile. AMT-562 exhibited deep antitumor response in both low-target expressing xenograft and heterogenous PDX models resistant to DXd-based ADC. It also produced a more durable response for responding tumors. AMT-562 showed higher synergy with both therapeutic antibodies and small-molecule inhibitors in combination therapies. AMT-562's improvement in broad tumor type bodes well for its ability to overcome resistance and expand responding patient populations beyond current HER3-targeting ADCs.

An ADC's functional performance is determined by the combination of its building blocks: the antibody, the linker, and the payload. The design of AMT-562 started with consideration of HER3 biology. Unlike HER2, HER3 is a tumor target with a lower abundance, multiple conformational states, and faster receptor endocytosis. For low-abundance antigens, a higher potency payload such as exatecan provides more effective therapeutic targeting. Ab562-HER3 binding was NRG1-independent and bound to either a more open or closed conformation, leading to broader and more effective targeting of HER3. In addition, Ab562 effectively inhibited HER3 signaling pathways in both the absence and presence of NRG1, reflecting that the naked antibody retained some functionality. Because of a relatively lower affinity, Ab562 caused a smaller (but still significant) decrease in cell surface HER3 expression and internalization than patritumab, potentially resulting in more accessible cell surface HER3 molecules by an ADC. Specific but moderate antibody-targeting binding might be a contributing factor in AMT-562's better efficacy, as suggested in previous studies for achieving higher tumor accumulation (40–42). Selecting exatecan as the payload and Ab562 as the HER-3 targeting antibody laid the foundation for a superior ADC design.

Among T moiety structures, T800 and T1000 were shown to generate stable, hydrophilic, and functional antibody-exatecan conjugates, although T800 was comparatively less hydrophilic due to the lack of pSAR (26). The highly hydrophilic Ab562 pairing with T800-exatecan produced equally homogeneous and hydrophilic ADCs with similar antitumor efficacy. However, AMT-562 displayed less organ toxicity in a non-human primate toxicity study than AMT-562-T1000, although both were well tolerated with a similar HNSTD as U3-1402. Pharmacokinetic measurements suggested that AMT-562 released payload exatecan faster and at a higher concentration. The reduced half-life of AMT-562 compared with AMT-562-T1000 may be responsible for AMT-562's lower toxicity because most dose-limiting ADC toxicities are now considered to be off-target and payload-related (43, 44). The higher stability and higher exposure levels of AMT-562-T1000 is likely the reason for the higher on target toxicity which seen in target organs in toxicity study. On the other hand, a less stable ADC structure rapidly releasing higher quantities of exatecan inside tumor cells may be beneficial for achieving higher antitumor efficacy (45). The totality of efficacy and safety considerations in selecting AMT-562 building components resulted in the final design of an optimized HER3-targeting ADC.

Similar to other T moiety–exatecan ADCs, AMT-562 displayed a superior pharmacologic profile characterized by faster and stronger intratumoral pharmacodynamic responses and deeper tumor cell penetration, resulting in higher antitumor potency. AMT-562 showed potent antitumor activity in representative digestive tumors including pancreatic, gastric, and colon cancer that were proven to be challenging for ADCs. ADCs including U3-1402/P-GGFG-DXd or 8201a/T-DXd have not shown efficacy in patients with colon cancer (22). In xenograft and clinically-relevant PDX models with MSS, or *BRAF-TP53* or *KRAS–TP53* double-mutant cells representative of unmet clinical needs, AMT-562 displayed high quality antitumor activity characterized by durable and CR. In comparison, P-GGFG-DXd was ineffective in many of the same models. A preliminary exploration of combination therapy showed that exatecan had a higher synergy with CHEK1 inhibitor compared to DXd, translating into improved synergistic antitumor efficacy of AMT-562 with CHEK1 inhibitor in comparison with P-GGFG-DXd. Combining ADCs based on Top I inhibitors with DNA-damaging pathway inhibitors may prove to be a general approach for better treatment outcomes (26, 46). AMT-562 displayed better synergy and more potent antitumor efficacy with anti-VEGF and anti-EGFR therapeutic antibodies that are standard-of-care for colon cancer. Ultimately, AMT-562 warrants further clinical investigation in patients with colon cancer, alone and in combination therapy.

In lung cancer, which U3-1402 has shown clinical efficacy against, AMT-562 showed better responses in NSCLC PDX models with different EGFR mutation mechanisms. AMT-562 was generally effective in low HER3 expression models and showed more durable response. Therefore, AMT-562 could potentially show improved efficacy against lung cancer with different resistance mechanisms. Furthermore, AMT-562 exhibited higher synergy and increased efficacy in combination with a TKI inhibitor or *KRAS* G12C inhibitor compared with P-GGFG-DXd. Our results highlighted AMT-562's potential to overcome lung cancer resistance, especially in U3-1402–insensitive patients that account for a majority of EGFR-TKI–resistant populations. With a recent demonstration of clinical resistance to *KRAS* G12C-EGFR inhibition due to the prevented suppression of ERK signaling in colon cancer (47), a combination of AMT-562 and KRAS inhibition may be an alternative strategy for overcoming similar resistance in lung cancer. It will be important to investigate the mechanism of observed combination effect in future studies.

In addition to U3-1402, EV20/NMS-P945 and EV20/MMAF are novel ADCs created by coupling an anti-HER-3 antibody EV20 with a DNA minor groove alkylating agent duocarmycin-like derivative through a peptidic cleavable linker and the tubulin polymerization

inhibitor monomethyl auristatin F through a noncleavable linker, respectively. Both ADCs show comparable activity to U3-1402 *in vitro* and *in vivo* tumor models. However, preliminary toxicity profiles in monkey and mouse showed much lower tolerance doses than U3-1402 despite using low DAR conjugation strategy (48, 49). Therefore, ADCs based on highly potent payloads are likely to have a more limited therapeutic window than Top I inhibitor–based ADCs.

In summary, we have designed and comprehensively characterized a HER3-targeting ADC that can potentially overcome the resistance of its DXd-counterpart P-GGFG-DXd (U3-1402) against a broad spectrum of HER3-positive tumors. Because AMT-562 displayed a favorable toxicity profile in non-human primates and similar HNSTD as U3-1402, the improved antitumor efficacy implies that AMT-562 has an enhanced therapeutic index. The consistent overexpression of HER3 in a substantial number of solid tumors makes HER3 a high-value ADC target. Demonstrated synergy of AMT-562 with other treatment options suggests a clinical strategy of combination therapy. AMT-562 has an opportunity to better realize the full potential of HER3 as a tumor antigen in broader tumor types than current ADCs and warrants clinical investigation in HER3-positive tumors.

Authors' Disclosures

S. Liu is a shareholder of Multitude Therapeutics. No disclosures were reported by the other authors.

Authors' Contributions

W. Weng: Resources, investigation, visualization, methodology. **T. Meng:** Conceptualization, resources, formal analysis, investigation, writing–review and editing. **J. Pu:** Investigation, visualization. **L. Ma:** Investigation, visualization. **Y. Shen:** Investigation, visualization. **Z. Wang:** Investigation, visualization. **R. Pan:** Investigation, visualization. **M. Wang:** Resources, validation, investigation, visualization. **C. Chen:** Investigation, visualization. **L. Wang:** Investigation, visualization. **J. Zhang:** Investigation, visualization. **B. Zhou:** Investigation, visualization. **S. Shao:** Investigation, visualization. **Y. Qian:** Investigation, visualization. **S. Liu:** Validation, investigation, visualization, writing–original draft, writing–review and editing. **W. Hu:** Validation, investigation, visualization, writing–original draft, writing–review and editing. **X. Meng:** Conceptualization, resources, formal analysis, supervision, validation, investigation, visualization, methodology, writing–original draft, project administration, writing–review and editing.

Acknowledgments

This study was funded by Multitude Therapeutics, Abmart, HySlink, Mabcare, Guangdong Provincial Key Laboratory of Chiral Molecule and Drug Discovery (2019B030301005). We want to thanks Y.F. Tang for supporting the clinical development of this project. We thank X. Meng for reading and editing the manuscript.

Note

Supplementary data for this article are available at Molecular Cancer Therapeutics Online (http://mct.aacrjournals.org/).

Received March 31, 2023; revised May 6, 2023; accepted June 6, 2023; published first June 11, 2023.

References

1. Campbell MR, Amin D, Moasser MM. HER3 comes of age: new insights into its functions and role in signaling, tumor biology, and cancer therapy. Clin Cancer Res 2010;16:1373–83.
2. Haikala HM, Janne PA. Thirty years of HER3: from basic biology to therapeutic interventions. Clin Cancer Res 2021;27:3528–39.
3. Mujoo K, Choi BK, Huang Z, Zhang N, An Z. Regulation of ERBB3/HER3 signaling in cancer. Oncotarget 2014;5:10222–36.
4. Olayioye MA, Neve RM, Lane HA, Hynes NE. The ErbB signaling network: receptor heterodimerization in development and cancer. EMBO J 2000;19:3159–67.
5. Ocana A, Vera-Badillo F, Seruga B, Templeton A, Pandiella A, Amir E. HER3 overexpression and survival in solid tumors: a meta-analysis. J Natl Cancer Inst 2013;105:266–73.
6. Sergina NV, Rausch M, Wang D, Blair J, Hann B, Shokat KM, et al. Escape from HER-family tyrosine kinase inhibitor therapy by the kinase-inactive HER3. Nature 2007;445:437–41.
7. Engelman JA, Zejnullahu K, Mitsudomi T, Song Y, Hyland C, Park JO, et al. MET amplification leads to gefitinib resistance in lung cancer by activating ERBB3 signaling. Science 2007;316:1039–43.
8. Erjala K, Sundvall M, Junttila TT, Zhang N, Savisalo M, Mali P, et al. Signaling via ErbB2 and ErbB3 associates with resistance and epidermal growth factor receptor (EGFR) amplification with sensitivity to EGFR inhibitor gefitinib in head and neck squamous cell carcinoma cells. Clin Cancer Res 2006;12:4103–11.
9. Aurisicchio L, Marra E, Roscilli G, Mancini R, Ciliberto G. The promise of anti-ErbB3 monoclonals as new cancer therapeutics. Oncotarget 2012;3:744–58.
10. LoRusso P, Janne PA, Oliveira M, Rizvi N, Malburg L, Keedy V, et al. Phase I study of U3–1287, a fully human anti-HER3 monoclonal antibody, in patients with advanced solid tumors. Clin Cancer Res 2013;19:3078–87.
11. Hill AG, Findlay MP, Burge ME, Jackson C, Alfonso PG, Samuel L, et al. Phase II study of the dual EGFR/HER3 inhibitor duligotuzumab (MEHD7945A) versus cetuximab in combination with FOLFIRI in second-line RAS wild-type metastatic colorectal cancer. Clin Cancer Res 2018;24:2276–84.
12. Drago JZ, Modi S, Chandarlapaty S. Unlocking the potential of antibody-drug conjugates for cancer therapy. Nat Rev Clin Oncol 2021;18:327–44.
13. Yonesaka K, Takegawa N, Watanabe S, Haratani K, Kawakami H, Sakai K, et al. An HER3-targeting antibody-drug conjugate incorporating a DNA topoisomerase I inhibitor U3–1402 conquers EGFR tyrosine kinase inhibitor-resistant NSCLC. Oncogene 2019;38:1398–409.
14. Hashimoto Y, Koyama K, Kamai Y, Hirotani K, Ogitani Y, Zembutsu A, et al. A novel HER3-targeting antibody-drug conjugate, U3–1402, exhibits potent therapeutic efficacy through the delivery of cytotoxic payload by efficient internalization. Clin Cancer Res 2019;25:7151–61.
15. Koganemaru S, Kuboki Y, Koga Y, Kojima T, Yamauchi M, Maeda N, et al. U3–1402, a novel HER3-targeting antibody-drug conjugate, for the treatment of colorectal cancer. Mol Cancer Ther 2019;18:2043–50.
16. Ueno S, Hirotani K, Abraham R, Blum S, Frankenberger B, Redondo-Muller M, et al. U3–1402a, a novel HER3-targeting ADC with a novel DNA topoisomerase I inhibitor, demonstrates a potent antitumor efficacy [abstract]. In: Proceedings of the American Association for Cancer Research Annual Meeting 2017; 2017 Apr 1–5; Washington, DC. Philadelphia (PA): AACR; Cancer Res 2017;77(13 Suppl): Abstract nr 3092.
17. Yonemori K, Masuda N, Takahashi S, Kogawa T, Nakayama T, Yamamoto Y, et al. Single agent activity of U3–1402, a HER3-targeting antibody-drug conjugate, in HER3-overexpressing metastatic breast cancer: updated results from a phase I/II trial. Ann Oncol 2019;30.
18. Yu HA, Baik CS, Gold K, Hayashi H, Johnson M, Koczywas M, et al. LBA62 efficacy and safety of patritumab deruxtecan (U3–1402), a novel HER3 directed antibody drug conjugate, in patients (pts) with EGFR-mutated (EGFRm) NSCLC. Ann Oncol 2020;31:S1189–S90.
19. Janne PA, Baik C, Su WC, Johnson ML, Hayashi H, Nishio M, et al. Efficacy and safety of patritumab deruxtecan (HER3-DXd) in EGFR inhibitor-resistant, EGFR-mutated non-small cell lung cancer. Cancer Discov 2022;12:74–89.
20. Hunter FW, Barker HR, Lipert B, Rothe F, Gebhart G, Piccart-Gebhart MJ, et al. Mechanisms of resistance to trastuzumab emtansine (T-DM1) in HER2-positive breast cancer. Br J Cancer 2020;122:603–12.
21. Ocana A, Amir E, Pandiella A. HER2 heterogeneity and resistance to anti-HER2 antibody-drug conjugates. Breast Cancer Res 2020;22:15.
22. Siena S, Di Bartolomeo M, Raghav KPS, Masuishi T, Loupakis F, Kawakami H, et al. A Phase II, multicenter, open-label study of trastuzumab deruxtecan (T-DXd; DS-8201) in patients (pts) with HER2-expressing metastatic colorectal cancer (mCRC): DESTINY-CRC01. J Clin Oncol 38:15s, 2020 (suppl; abstr 4000).

23. Yamaguchi K, Bang YJ, Iwasa S, Sugimoto N, Ryu MH, Sakai D, et al. Trastuzumab deruxtecan (T-DXd; DS-8201) in patients with HER2-low, advanced gastric or gastroesophageal junction (GEJ) adenocarcinoma: results of the exploratory cohorts in the phase II, multicenter, open-label DESTINY-Gastric01 study. Ann Oncol 2020;31:S899–900.
24. Chu CE, Sjostrom M, Egusa EA, Gibb EA, Badura ML, Zhu J, et al. Heterogeneity in NECTIN4 expression across molecular subtypes of urothelial cancer mediates sensitivity to enfortumab vedotin. Clin Cancer Res 2021;27:5123–30.
25. Gil V, Miranda S, Riisnaes R, Gurel B, D'Ambrosio M, Vasciaveo A, et al. HER3 is an actionable target in advanced prostate cancer. Cancer Res 2021;81:6207–18.
26. Weng W, Meng T, Zhao Q, Shen Y, Fu G, Shi J, et al. Antibody-exatecan conjugates with a novel self-immolative moiety overcome resistance in colon and lung cancer. Cancer Discov 2023;13:950–73.
27. Joto N, Ishii M, Minami M, Kuga H, Mitsui I, Tohgo A. DX-8951f, a water-soluble camptothecin analog, exhibits potent antitumor activity against a human lung cancer cell line and its SN-38-resistant variant. Int J Cancer 1997;72:680–6.
28. Thakkar D, Sancenon V, Taguiam MM, Guan S, Wu Z, Ng E, et al. 10D1F, an anti-HER3 antibody that uniquely blocks the receptor heterodimerization interface, potently inhibits tumor growth across a broad panel of tumor models. Mol Cancer Ther 2020;19:490–501.
29. Romaniello D, Marrocco I, Belugali Nataraj N, Ferrer I, Drago-Garcia D, Vaknin I, et al. Targeting HER3, a catalytically defective receptor tyrosine kinase, prevents resistance of lung cancer to a third-generation EGFR kinase inhibitor. Cancers 2020;12:2394.
30. Schoeberl B, Faber AC, Li D, Liang MC, Crosby K, Onsum M, et al. An ErbB3 antibody, MM-121, is active in cancers with ligand-dependent activation. Cancer Res 2010;70:2485–94.
31. Yonesaka K, Hirotani K, Kawakami H, Takeda M, Kaneda H, Sakai K, et al. Anti-HER3 monoclonal antibody patritumab sensitizes refractory non-small cell lung cancer to the epidermal growth factor receptor inhibitor erlotinib. Oncogene 2016;35:878–86.
32. Khera E, Dong S, Huang H, de Bever L, van Delft FL, Thurber GM. Cellular-resolution imaging of bystander payload tissue penetration from antibody-drug conjugates. Mol Cancer Ther 2022;21:310–21.
33. Chen SH, Zhang Y, Van Horn RD, Yin T, Buchanan S, Yadav V, et al. Oncogenic BRAF deletions that function as homodimers and are sensitive to inhibition by RAF dimer inhibitor LY3009120. Cancer Discov 2016;6:300–15.
34. Piawah S, Venook AP. Targeted therapy for colorectal cancer metastases: a review of current methods of molecularly targeted therapy and the use of tumor biomarkers in the treatment of metastatic colorectal cancer. Cancer 2019;125:4139–47.
35. Jaaks P, Coker EA, Vis DJ, Edwards O, Carpenter EF, Leto SM, et al. Effective drug combinations in breast, colon and pancreatic cancer cells. Nature 2022;603:166–73.
36. Uchibori K, Inase N, Araki M, Kamada M, Sato S, Okuno Y, et al. Brigatinib combined with anti-EGFR antibody overcomes osimertinib resistance in EGFR-mutated non-small-cell lung cancer. Nat Commun 2017;8:14768.
37. Shaw AT, Ou SH, Bang YJ, Camidge DR, Solomon BJ, Salgia R, et al. Crizotinib in ROS1-rearranged non-small-cell lung cancer. N Engl J Med 2014;371:1963–71.
38. Haikala HM, Köhler J, Lopez T, Eser P, Xu M, Yu C, et al. EGFR inhibition enhances the cellular uptake and antitumor activity of the novel HER3 antibody drug conjugate U3–1402 [abstract]. In: Proceedings of the Annual Meeting of the American Association for Cancer Research 2020; 2020 Apr 27–28 and Jun 22-24. Philadelphia (PA): AACR; Cancer Res 2020;80(16 Suppl):Abstract nr 5192.
39. Yonesaka K, Tanizaki J, Maenishi O, Haratani K, Kawakami H, Tanaka K, et al. HER3 augmentation via blockade of EGFR/AKT signaling enhances anticancer activity of HER3-targeting patritumab deruxtecan in EGFR-mutated non-small cell lung cancer. Clin Cancer Res 2022;28:390–403.
40. Rudnick SI, Lou J, Shaller CC, Tang Y, Klein-Szanto AJ, Weiner LM, et al. Influence of affinity and antigen internalization on the uptake and penetration of anti-HER2 antibodies in solid tumors. Cancer Res 2011;71:2250–9.
41. Wong OK, Tran TT, Ho WH, Casas MG, Au M, Bateman M, et al. RN765C, a low affinity EGFR antibody drug conjugate with potent anti-tumor activity in preclinical solid tumor models. Oncotarget 2018;9:33446–58.
42. Tsumura R, Manabe S, Takashima H, Koga Y, Yasunaga M, Matsumura Y. Influence of the dissociation rate constant on the intra-tumor distribution of antibody-drug conjugate against tissue factor. J Control Release 2018;284:49–56.
43. Masters JC, Nickens DJ, Xuan D, Shazer RL, Amantea M. Clinical toxicity of antibody drug conjugates: a meta-analysis of payloads. Invest New Drugs 2018;36:121–35.
44. Saber H, Simpson N, Ricks TK, Leighton JK. An FDA oncology analysis of toxicities associated with PBD-containing antibody-drug conjugates. Regul Toxicol Pharmacol 2019;107:104429.
45. Kopp A, Hofsess S, Cardillo TM, Govindan SV, Donnell J, Thurber GM. Antibody-drug conjugate sacituzumab govitecan drives efficient tissue penetration and rapid intracellular drug release. Mol Cancer Ther 2023;22:102–11.
46. Kinneer K, Wortmann P, Cooper ZA, Dickinson NJ, Masterson L, Cailleau T, et al. Design and preclinical evaluation of a novel B7-H4-directed antibody-drug conjugate, AZD8205, alone and in combination with the PARP1-selective inhibitor AZD5305. Clin Cancer Res 2023;29:1086–101.
47. Yaeger R, Mezzadra R, Sinopoli J, Bian Y, Marasco M, Kaplun E, et al. Molecular characterization of acquired resistance to KRASG12C-EGFR inhibition in colorectal cancer. Cancer Discov 2023;13:41–55.
48. Capone E, Lattanzio R, Gasparri F, Orsini P, Rossi C, Iacobelli V, et al. EV20/NMS-P945, a novel thienoindole based antibody-drug conjugate targeting HER-3 for solid tumors. Pharmaceutics 2021;13:483.
49. Capone E, Lamolinara A, D'Agostino D, Rossi C, De Laurenzi V, Iezzi M, et al. EV20-mediated delivery of cytotoxic auristatin MMAF exhibits potent therapeutic efficacy in cutaneous melanoma. J Control Release 2018;277:48–56.